PCCP

PAPER

View Article Online
View Journal | View Issue

Cite this: *Phys. Chem. Chem. Phys.*, 2017, **19**, 1010

Polar solvent fluctuations drive proton transfer in hydrogen bonded complexes of carboxylic acid with pyridines: NMR, IR and *ab initio* MD study†

B. Koeppe,[a] S. A. Pylaeva,[b] C. Allolio,[b] D. Sebastiani,*[b] E. T. J. Nibbering,*[c] G. S. Denisov,[d] H.-H. Limbach[e] and P. M. Tolstoy*[f]

Received 28th September 2016,
Accepted 2nd December 2016

DOI: 10.1039/c6cp06677a

www.rsc.org/pccp

We study a series of intermolecular hydrogen-bonded 1:1 complexes formed by chloroacetic acid with 19 substituted pyridines and one aliphatic amine dissolved in CD_2Cl_2 at low temperature by ^1H and ^{13}C NMR and FTIR spectroscopy. The hydrogen bond geometries in these complexes vary from molecular (O–H···N) to zwitterionic ($O^-\cdots H-N^+$) ones, while NMR spectra show the formation of short strong hydrogen bonds in intermediate cases. Analysis of C=O stretching and asymmetric CO_2^- stretching bands in FTIR spectra reveal the presence of proton tautomerism. On the basis of these data, we construct the overall proton transfer pathway. In addition to that, we also study by use of *ab initio* molecular dynamics the complex formed by chloroacetic acid with 2-methylpyridine, surrounded by 71 CD_2Cl_2 molecules, revealing a dual-maximum distribution of hydrogen bond geometries in solution. The analysis of the calculated trajectory shows that the proton jumps between molecular and zwitterionic forms are indeed driven by dipole–dipole solvent–solute interactions, but the primary cause of the jumps is the formation/breaking of weak CH···O bonds from solvent molecules to oxygen atoms of the carboxylate group.

1. Introduction

Proton tautomerism in hydrogen bonds (H-bonds) is a well-established phenomenon and a thoroughly studied subject, notably for H-bonded systems in liquid solutions, with a significant number of publications based on optical[1–8] and NMR spectroscopy.[9–15]

The experimental data are often discussed in terms of a tautomeric equilibrium between two fixed states. This implies that in a series of changing external conditions or a series of homologous complexes the proton transfer pathway occurs as shown in Fig. 1a, where each row corresponds to a particular system (or a set of external conditions), characterized by a certain value of equilibrium constant *K*. Alternatively, the same information can be depicted as a series of double-well potential energy surfaces (PES) of various degrees of asymmetry for the bridging proton motion. However, in many cases NMR has shown the formation of complexes with strong H-bonds, which are characterized by a quasi-symmetric position of the proton.[16–18] This leads to a scheme shown in Fig. 1b, which can be characterized by a series of single-well proton potentials with the changing position of the minimum ("mesomeric" scheme, in contrast to the tautomeric one). In the gas phase, a tautomeric equilibrium between molecular and zwitterionic forms of a complex has not been observed before. Instead, in a series of works based on rotation spectra of hydrogen halide–amine complexes a "mesomeric" proton transfer pathway was shown.[19] The IR spectra of the same systems embedded in noble gas cryo-matrices have indicated that upon increase of the polarizability of matrix atoms a molecular complex gradually turns into a zwitterionic one.[20] In recent years, attempts were made to combine tautomeric and mesomeric views into one, resulting in a model which is illustrated in Fig. 1c.[14,15,21,22] Here, a tautomeric shift of the equilibrium is accompanied by a mesomeric change of the structures of the individual tautomers.

It also has been demonstrated that a crucial role is played by the thermal fluctuations of the solvent molecules in the proximity of the complex.[23–25] The coupling of the bridging proton motion to the solvation shell configuration (solvent coordinate) is schematically shown in Fig. 2: at each horizontal cut (fixed solvent coordinate) the light bridging proton adjusts its position in a corresponding single-well potential. As a result, the "double-well"

[a] *Department of Chemistry, Humboldt-Universität zu Berlin, Germany*
[b] *Institute of Chemistry, Martin-Luther Universität Halle-Wittenberg, Germany. E-mail: daniel.sebastiani@chemie.uni-halle.de*
[c] *Max Born Institut für Nichtlineare Optik und Kurzzeitspektroskopie, Berlin, Germany. E-mail: nibberin@mbi-berlin.de*
[d] *Department of Physics, St.Petersburg State University, Russia*
[e] *Institute of Chemistry and Biochemistry, Freie Universität Berlin, Germany*
[f] *Center for Magnetic Resonance, St. Petersburg State University, Russia. E-mail: peter.tolstoy@spbu.ru*

† Electronic supplementary information (ESI) available. See DOI: 10.1039/c6cp06677a

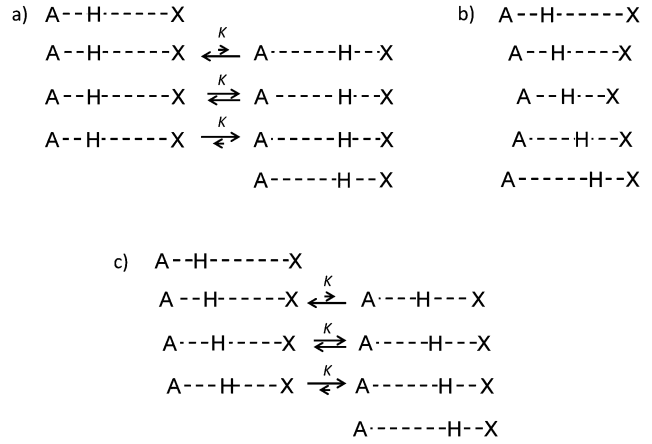

Fig. 1 Schemes of the bridging proton transfer pathways for hypothetical series of complexes with intermolecular H-bonds in solution: (a) tautomeric equilibrium: (b) continuous ("mesomeric") proton transfer and (c) combined scheme, where two-state tautomerism is combined with the continuous shift of proton positions in each individual tautomer.

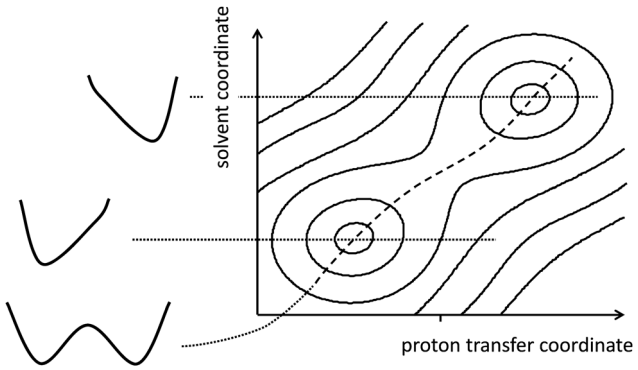

Fig. 2 Schematic representation of the proton transfer pathway for a hydrogen bonded complex in liquid solution. Proton coordinate adjusts to the solvent coordinate and the double-well potential is realized along the coordinate including solvent motion.

proton potential is realized along the combined coordinate shown as dashed line. Perhaps the most notable feature in Fig. 2 is that each tautomer is represented not by a single structure, but by an ensemble of "solvatomers", the notion which was recently confirmed by *ab initio* molecular dynamics simulations (*ab initio* MD) of an $(OHO)^-$-bonded system.[24] In this approach the two-state model of tautomerism is an approximation, substituted by the whole proton distribution function.

Intermolecular OHN-bonded complexes formed by carboxylic acids and various nitrogen bases (pyridines, amines *etc.*) can be considered as one of the classical objects for H-bond research. Carboxylic acids and nitrogen bases readily form 1 : 1 complexes that can be quite strong[26,27] and display a range of H-bond geometries. Previously, some of us have established several NMR hydrogen bond correlations for OHN complexes, using ^1H and ^{15}N NMR chemical shifts, $^1J_{NH}$ coupling constant, carboxylic carbon ^{13}C NMR chemical shift, H/D isotope effects on all of the above-mentioned parameters as well as the value of ^{15}N–^2H dipole–dipole coupling constant (for complexes in solid state).[9,17,28–32] These correlations aimed to connect gradual changes in experimental NMR parameters with gradual changes in the average H-bond geometry expressed *via* linear combinations of interatomic distances $q_1 = 1/2(r_{OH} - r_{HN})$ and $q_2 = r_{OH} + r_{HN}$. It should be noted that q_1 and q_2 themselves are correlated, as was shown for various types of H-bonded complexes by neutron diffraction:[33,34] shortening of the O···N distance (q_2 decrease) is accompanied by the symmetrization of the H-bond ($|q_1|$ decrease). While NMR hydrogen bond correlations proved to be quite useful and reliable,[35] the problem of possible proton tautomerism within the complex, *i.e.* O–H···N ⇌ O^-···H–N^+, was addressed in NMR studies only occasionally by us[9] (see also early works in ref. 8, 36 and 37) and other work groups.[12] In the case of a fast proton tautomerism between the molecular and the zwitterionic forms, every experimentally observed NMR parameter becomes a weighted-average over two intrinsic values. As a result, it is often difficult to distinguish the spectral manifestations of the proton displacement in the H-bond and the shift of the tautomeric equilibrium.

In the IR spectroscopic studies the possibility of proton tautomerism in carboxylic acid/pyridine complexes has been known and explored for a long time.[1–4,9] The IR spectral bands of individual isomers can be observed independently[5] or as part of the overall inhomogeneously broadened band.[6,7] However, despite widely acclaimed success in correlating some IR spectroscopic observables with the H-bond geometry (see for example correlation of ν_{OH} stretching frequency with the O···O distance,[38–41] or with the O···N distance[42]) the underlying microscopic mechanisms for the parameter value spread in these correlation plots have remained an issue for continued research, being either of intramolecular nature or caused by surroundings effects (in particular electric fields). Ultrafast infrared 2D-IR and pump–probe spectroscopy has provided key insight into the degree of inhomogeneous broadening and spectral diffusion of disordered H-bond networks,[43] in particular water as a liquid[44–48] and as hydrating agent,[49–53] and of the role of anharmonic couplings of low-frequency H-bond modulation modes and of Fermi resonances of fingerprint vibrations (in particular OH or NH bending) with OH and NH stretching vibrations in medium strong H-bonds.[54,55] Recently femtosecond IR pump–probe experiments have elucidated the ultrafast nature of the electrical fields imposed by the fluctuating polar solvent on the proton transfer coordinate of the Zundel cation $H_5O_2^+$.[56] For OHN-bonded complexes much less is established. The relative importance of the intrinsic H-bond strength and the coupling with the polar solvent has been explored for aromatic alcohol–acetonitrile complexes, where the OHN hydrogen bond can be categorized as weak, even – for 2-naphthol – in the electronic excited state.[57] For strong (short) OHN-bonded complexes other IR marker modes have been explored in a limited number of studies.[58,59]

As mentioned above, the gradual geometric shift and tautomeric equilibrium are not mutually exclusive. By using combined NMR/UV-vis setup designed by some of us[60] we have recently demonstrated on the example of $(OHO)^-$ hydrogen bonded complexes formed by 2-chloro-4-nitrophenol and a series of

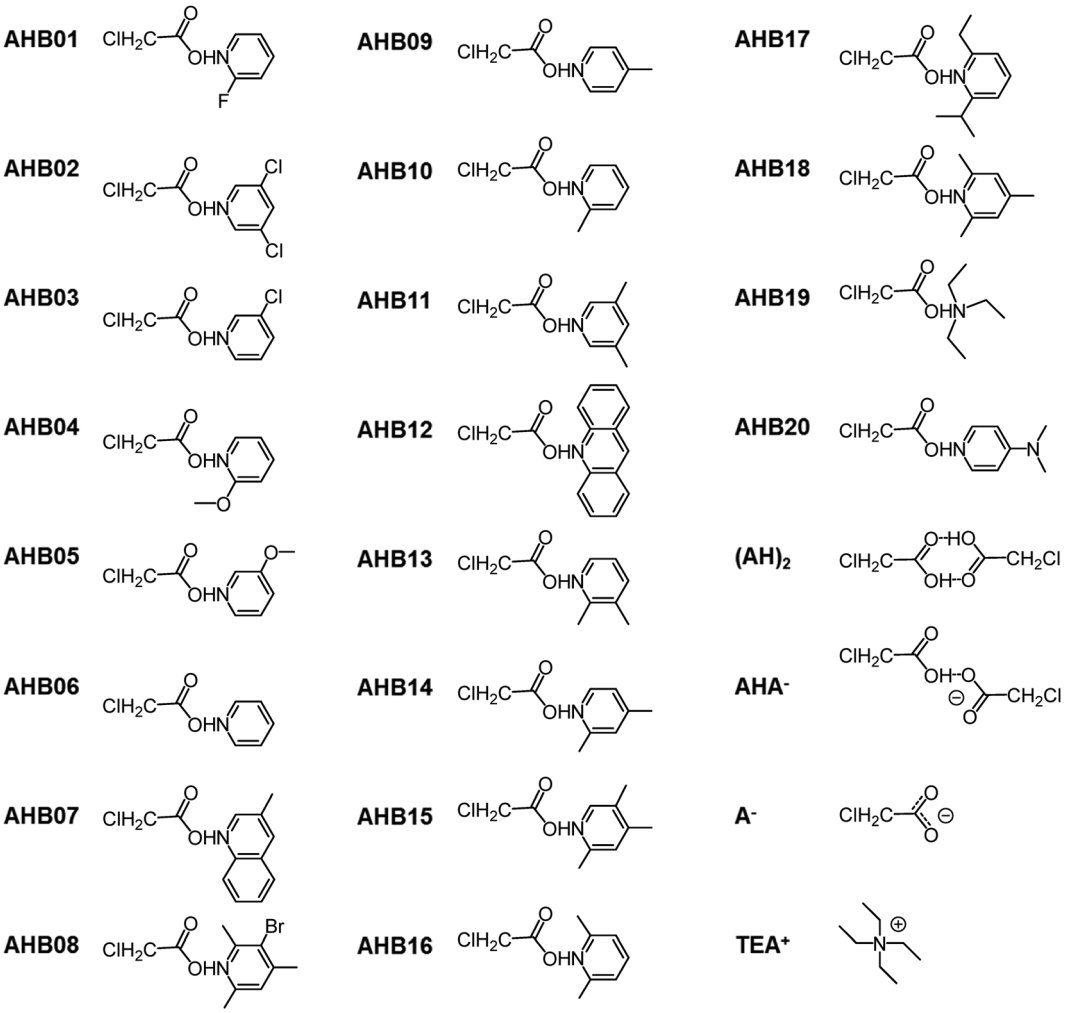

Fig. 3 Schematic representation of the complexes **AHB01**–**AHB20** of chloroacetic acid and N-bases studied in this work. Chloroacetic acid self-associates **(AH)$_2$**, **AHA**$^-$, anion **A**$^-$ and counter-cation tetraethylammonium (**TEA**$^+$) for charged complexes are shown as well. In all cases, the hydrogen bond geometries are shown formally simply as "OHN" and "OHO", without implying a particular bridging proton position.

carboxylates that the proton transfer pathway as shown in Fig. 1c is being realized in a polar aprotic solution. The tautomerism itself, the role of the counter-cation and the role of solvent molecules' dynamics in driving the bridging proton motion have been confirmed by *ab initio* MD simulations.[24] While in the combined spectroscopy NMR and UV-vis spectra were recorded simultaneously and the resulting spectral information was perfectly consistent (allowing for 2D correlations plots[61]), it is possible to obtain NMR and optical data independently. In this work we expand this line of research into the area of OHN-bonded complexes and NMR/IR spectra.[62] We revisit the question of the proton transfer pathway and the solvent–solute coupling on the example of intermolecular complexes of carboxylic acid and nitrogen bases dissolved in polar aprotic medium. For this study we have selected 20 complexes formed by chloroacetic acid with nitrogen bases (19 pyridines and 1 amine), as well as some self-associates of chloroacetic acid, dissolved in CD_2Cl_2 (CH_2Cl_2) at 170–300 K.

All studied complexes are depicted in Fig. 3 and labeled **AHB01**–**AHB20** for OHN-bonded complexes, **(AH)$_2$**, **AHA**$^-$ and **A**$^-$ for the cyclic dimer, the homo-conjugated anion and the anion of chloroacetic acid, respectively. The counter-cation used for anionic systems was tetraethylammonium, labeled **TEA**$^+$ in Fig. 3. As one of our goals is to determine the H-bond geometries, in Fig. 3 we avoid showing the proton position. As main spectroscopic observables we have selected ^{1}H and ^{13}C NMR chemical shifts, as well as frequencies of ^{12}C═O and ^{13}C═O stretching bands in IR spectra. Carbonyl stretching vibrations are often used as marker modes for H-bonded complexes of carboxylic acids, because such bands are intensive and are located in the frequency range relatively free from other strong contributions.[63] Ring modes of pyridines and OH stretching modes of the acid appeared to be less informative and will be mentioned only briefly in the text. Changing the base in the series **AHB01**–**AHB20** served as a way to change the geometry of the system (and/or equilibrium constant of the tautomerism), while changing the temperature served as a way to change the properties of the solvation shell and *via* this the structure of the complex as well. The interaction of the polar aprotic medium with a system exhibiting high atomic polarizability and potentially large dipole

moment is expected to be substantial. In order to look at the system in atomistic detail we have chosen one of the complexes, namely, the complex of chloroacetic acid with 2-methylpyiridine (**AHB10**), and have studied it with *ab initio* MD. This method allowed us to investigate H-bond dynamics and also to study weak specific solvent–solute interactions.

The main questions which we address in this paper are as follows. Which of the proton transfer pathways shown in Fig. 1 applies to the studied systems? How well does the two-state model represent the situation? In case of proton tautomerism, what exactly drives the proton motion back and forth? Besides, we want to correlate the $\nu_{C=O}$ frequency of chloroacetic acid with the hydrogen bond geometry.

2. Experimental

All samples studied in this work are dichloromethane (CH_2Cl_2 or CD_2Cl_2) solutions. CH_2Cl_2 (Merck, amylene stabilized) and CD_2Cl_2 (99.8%, Deutero GmbH) were dried by molecular sieves (4 Å). 3-bromo-2,4,6-collidine was synthesized from 2,4,6-collidine by Andrey Gurinov by the procedure described in ref. 64.

All other chemicals were obtained commercially (Alfa Aesar, Aldrich) and used without further processing. Samples were obtained from dichloromethane stock solutions of acids and bases (0.2–0.5 M) using microliter pipettes.

2.1 Tetraethylammonium salts of chloroacetic acid

0.10 mL chloroacetic acid solution (0.20 M in MeOH) were mixed with 0.19 mL tetraethylammonium hydroxide (TEAOH) solution (0.10 M in methanol) and the solvent was evaporated in vacuum. The residue was dried by addition of a small amount of dry CH_2Cl_2 and subsequent vacuum evaporation (repeated twice). Finally, the residue was taken up in 0.5 mL of CH_2Cl_2 (0.04 M TEA chloroacetate) and FTIR spectra of this solution were recorded before and after each addition of sub molar equivalent amounts of chloroacetic acid as 0.20 M CH_2Cl_2 solution. After cumulated addition of 0.6 and 0.8 equivalents for natural abundance and 1-^{13}C-labeled acids, respectively, the solution was diluted by addition of 0.5 mL CH_2Cl_2 and of the resulting solution (0.02 M TEA chloroacetate) variable temperature FTIR spectra were acquired.

2.2 Pyridine complexes of chloroacetic acid

Concentration of chloroacetic acid typically was 0.03 M. Base concentrations were equal or higher and optimized empirically starting from close to 1 : 1 ratio, using ^{1}H NMR spectra recorded at *ca.* 180 K as the criterion. It was found that, on the one hand, high base concentrations ensure selectivity of formation of 1 : 1 acid–base complexes in exclusion of, for example, 2 : 1 complexes, while too high excess of base led to significant broadening and upfield shifts of bridging proton NMR signal, possibly due to signal averaging with increasing amount of residual water. Optimum acid/base ratio varied between almost 1 : 4 and 1 : 1 for weak to strong bases. In case of **AHB20**, resolving the complexes' ^{13}C NMR signals required much higher base concentration (1 : 5) than the 1 : 1 optimum for proton spectra. For FTIR isotope difference spectra of pairs of samples containing a CD_2Cl_2 solution of a pyridine derivative and either chloroacetic acid in natural isotope abundance or 1-^{13}C-chloroacetic acid (99%) were prepared under ^{1}H NMR monitoring such that acid/base ratio differed by not more than 5%.

2.3 NMR and FTIR spectroscopic experiments

Samples for the measurement of ^{1}H and ^{13}C NMR spectra were obtained from the same CD_2Cl_2 solutions as used for preparing the samples for FTIR. NMR spectra were recorded at about 170 K using thin wall samples tubes and a probe optimized for ^{13}C detection. Spectra were calibrated to $\delta(C\underline{H}DCl_2)$ = 5.32 ppm and $\delta(^{13}\underline{C}D_2Cl_2)$ = 53.5 ppm, respectively. FTIR spectra were recorded with a Varian 640 FTIR spectrometer equipped with a vacuum cryostat (Specac Ltd). Sample solutions were contained between CaF_2 windows (1 × 20 mm^2) and 0.2 mm PTFE spacers, tightly pressed together by home-made sample holders, keeping losses to surrounding vacuum to a minimum. Raw absorption data was acquired against blank reference. Subtraction of temperature specific solvent spectra and compensation for residual gases (CO_2, H_2O) was performed in subsequent processing. Isotope difference spectra were obtained from individually processed spectra; scaling was adjusted to optimum cancellation of invariant spectral components. Further data treatment is described in Results.

2.4 Computational details

We performed *ab initio* MD simulation of the solvated complex using the CP2K simulation package.[65] We chose GPW method,[66] the BLYP-D2 DFT functional[67–69] together with a TZVP basis on all atoms with the exception of oxygen and hydrogen, for which an aug-TZV2P/TZV2P basis sets were used, respectively. The plane-wave cutoff was set to 350 Ry. We used GTH pseudopotentials for all atoms.[70] The simulations were performed in an *NVT* ensemble at 300 K using a CSVR thermostat[71] with a time constant of 100 fs. All hydrogen atoms were simulated as deuterium atoms, which allowed us to increase the time step to 1 fs; from now on we will refer to them as "protons" for convenience. The employed SCF convergence was 10^{-8} a.u. The molecular dynamics was done in a cubic periodic box with a side length of 20 Å. The initial geometry of the complex was optimized in gas phase using Gaussian09.[72] Then the complex was inserted in previously equilibrated solvent box by calculating the molecular volume of the overlapping van der Waals radii of its atoms and removing the equivalent volume of DCM molecules calculated in the same way. Simulation was then performed for the complex surrounded by 71 DCM molecules for 31 ps: 26 ps were used for data sampling after 5 ps of equilibration. We used VMD[73] and TRAVIS[74] for trajectory analysis.

Chemical shifts were calculated in Gaussian09 at PBE0/IGLO-III[75–78] level of theory for a set of 98 random snapshots extracted from the trajectory. All solvent molecules within 3.3 Å range from the complex were taken into account. Isotropic magnetic shieldings were referenced to tetramethylsilane

(^{1}H and ^{13}C) and to 2-methylpyridine (^{15}N) calculated at the same level of theory.

3. Results

Parts of NMR and IR spectra of a subset of the studied complexes, **AHB01** through **AHB20** of chloroacetic acid with pyridines (see Fig. 3) are shown in Fig. 4 and 5, respectively. The complete sets of spectra are given in Fig. S1–S10 in ESI.†

Parameters of the complete set of complexes **AHB01**–**AHB20** for the temperature *ca.* 170 K are summarized in Table 1 and for other temperatures in Table S1 of ESI.† Aiming at ordering the complexes by degree of proton transfer, we took the bases' pK_a values as initial guideline, but made some minor changes to this order when adopting the chemical shift δ(C2) (chloromethyl carbon atom) of the chloroacetic acid moiety as the preferred criterion. This choice will be justified below.

3.1. NMR spectra

Fig. 4a shows the successive down- and up-field trends of the bridging proton chemical shifts characteristic of proton transfer through the center of the hydrogen bond. Interestingly, this coincides with the monotonic downfield shift of the C2 resonances of the chloroacetic acid moieties shown in Fig. 4c that we used to define the order of spectra. Conversely, the C1 signals in Fig. 4b follow the monotonic downfield trend of the C2 signals only within the first half of the pathway.

For further elucidation, plots of just discussed NMR parameters for the complete set of systems studied are given in Fig. 6. Fig. 6a and b show the chemical shifts of the hydrogen bonding proton *vs.* δ(C1) and δ(C2), respectively. In Fig. 6c, the pK_a(**BH$^+$**) values of the bases in aqueous solution, taken from literature, are plotted *vs.* δ(C2). Carbon chemical shifts of the chloroacetate anion (tetraethylammonium salt) are represented by vertical dashed lines marked "A$^-$". Dotted lines indicate possible correlated changes of spectral parameters of complexes along the proton transfer coordinate (hand drawn guides for the eye).

Considering Fig. 6a and b we note that within the initial stages of proton transfer from O to N, both δ(C1) and δ(C2) increase monotonically. While for δ(C2) this trend seems to continue within zwitterionic complexes, no further increase in δ(C1) is observed and, in fact, δ(C1) seems to even slightly decline again on the far end of the pathway.[31] Even though statements on that region are complicated by the scarcity of experimental data on corresponding **AHB** complexes, this view seems to be confirmed by considering data of the chloroacetate anion which should constitute the limiting case of full proton transfer: while δ(C2) of tetraethylammonium chloroacetate exceeds all values found for **AHB** complexes, its δ(C1) signal falls behind all the respective data. In Fig. 6c, we find that δ(C2) displays a clear sigmoidal correlation with pK_a(**BH$^+$**) (similar sigmodial dependencies on pK_a for the hydrogen bonded complexes with increasing degree of proton transfer have been previously observed for various parameters by IR and NQR, see f.e. ref. 80).

Finally, a comment to the open square data points in the plots of Fig. 6 corresponding to **AHB19** (the triethylamine complex) which constitutes a significant outlier both in Fig. 6b and c. Both the bridging proton chemical shift for **AHB19** of *ca.* 13.4 ppm as well as pK_a(**B19H$^+$**) $\approx$10.8 seem to suggest that triethylamine is by far the strongest proton acceptor of the series much rather than **B20** (4-dimethylaminopyridine) whose complex **AHB20** shows the highest δ(C2). However, both the low proton chemical shift for **AHB19** and the high pK_a of **B19H$^+$** are probably misleading: triethylamine is the only aliphatic base of the series which leads to two considerations. Firstly, proton chemical shifts

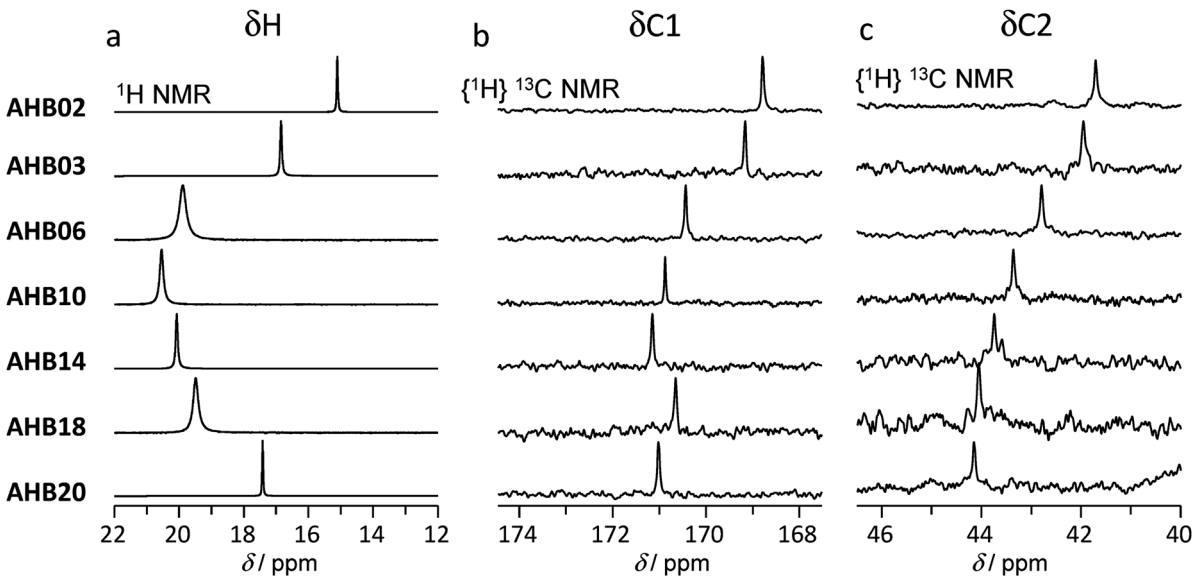

Fig. 4 Parts of ^{1}H and ^{13}C NMR spectra of samples, containing chloroacetic acid and various N-bases in CD_2Cl_2 solution, measured at *ca.* 170 K. Out of the complete set of complexes (**AHB01**–**AHB20**) only several have been selected as a representative subset.

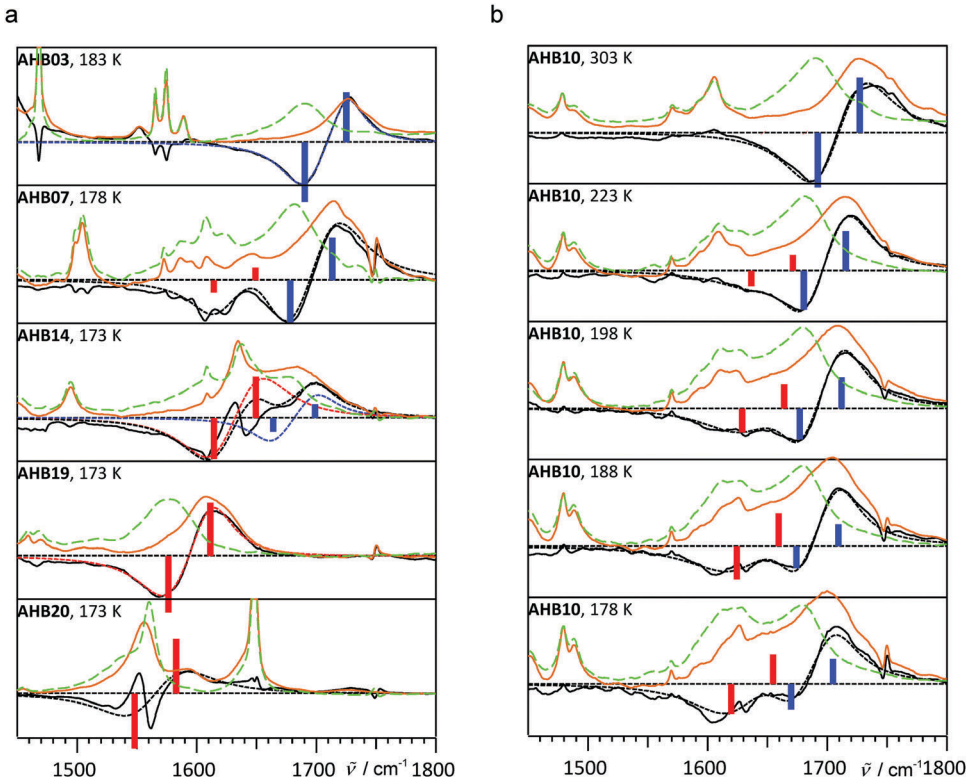

Fig. 5 Parts of IR spectra in the region of C=O stretching vibration of samples, containing chloroacetic acid and various N-bases in CH_2Cl_2 solution, measured at around 180 K (exact temperature are given in the figure) for complexes **AHB03**, **AHB07**, **AHB14**, **AHB19** and **AHB20** (a) and at various temperatures for **AHB10** complex (b). Spectra of the complexes containing ^{13}C-labelled chloroacetic acid are shown as green traces (long dashes), complexes containing non-labelled acid are shown as solid orange traces. Black solid traces correspond to the isotope difference spectra (the spectrum of ^{13}C-labelled species minus the spectrum of non-labelled species). Blue, red and black dotted traces correspond to the result of the fitting, as described in the Discussion section.

Table 1 Properties of chloroacetic acid base complexes **AHB**. Definition of bases **B01** to **B20**, pK_a values of conjugated bases $\mathbf{BH^+}$,[79] molar ratio n_B/n_{AH} in NMR samples. Spectral parameters obtained at *ca.* 170 K in dichloromethane solution: chemical shifts δ (in ppm) of hydrogen bonding protons (H), and chloroacetic acid nuclei H2, C1, and C2. IR parameters determined at given temperatures T: vibrational frequency $\tilde{\nu}$ and band width $\Delta\tilde{\nu}$ (both in cm^{-1}) of the carbonyl stretching and asymmetric carboxylate stretching vibrations of the ^{12}C isotopologs of neutral and anionic acid moieties, respectively; fractional integrated intensity x_{red} of the band of the latter of the two modes

									$\tilde{\nu}(^{12}C{=}O)$ ("blue")		$\tilde{\nu}_{as}(^{12}CO_2^-)$ ("red")		
Complex	Base **B**	p$K_a(\mathbf{BH^+})$	n_B/n_{AH}	δ(H)	δ(H2)	δ(C1)	δ(C2)	T/K	$\tilde{\nu}$	$\Delta\tilde{\nu}$	$\tilde{\nu}$	$\Delta\tilde{\nu}$	x_{red}
AHB01	2-Fluoropyridine	−0.44	2.6	14.58	4.25	168.57	41.64		n.d.[a]				
AHB02	3,5-Dichloropyridine	0.71	3.2	15.11	4.23	168.79	41.71	178	1730	28[b]			0
AHB03	3-Chloropyridine	2.81	3.5	16.85	4.22	169.17	41.95	183	1725	38			0
AHB04	2-Methoxypyridine	3.28	2.0	16.79	4.22	169.09	42.07		n.d.				
AHB05	3-Methoxypyridine	4.78	2.4	19.34	4.19	170.12	42.59	178	1719	47			0
AHB06	Pyridine	5.23	1.4	19.88	4.18	170.44	42.79	188	1717	49	1645	62	0.13
AHB07	3-Methylquinoline	5.7	1.3	20.36	4.25	171.08	42.89	178	1713	66	1649	50	0.23
AHB08	3-Bromo-2,4,6-collidine	4.96	2.7	19.80	4.14	170.13	43.10		n.d.				
AHB09	4-Picoline	5.99	1.0	20.42	4.14	170.95	43.27	188	1708	46	1651	74	0.59
AHB10	2-Picoline	6.00	1.3	20.54	4.14	170.88	43.35	178	1705	53	1655	81	0.54
AHB11	3,5-Lutidine	6.15	1.2	20.47	4.13	171.08	43.37		n.d.				
AHB12	Acridine	5.58	1.4	20.77	4.32	170.73	43.42		n.d.				
AHB13	2,3-Lutidine	6.57	1.1	20.38	4.12	171.08	43.68	173	1699	47	1645	74	0.77
AHB14	2,4-Lutidine	6.63	1.1	20.07	4.11	171.15	43.74	173	1699	46	1650	65	0.75
AHB15	2,3,5-Collidine	6.53	1.1	19.84	4.11	171.19	43.85	183	1696	33	1640	79	0.90
AHB16	2,6-Lutidine	6.65	1.0	20.19	4.10	170.65	43.87	188	1684	80	1634	80	0.75
AHB17	2-Ethyl-6-isopropyl-pyr.		1.3	20.03	4.11	170.71	43.92	178	1670	80	1624	80	0.71
AHB18	2,4,6-Collidine	7.43	1.0	19.49	4.07	170.65	44.05	173	1746	80	1617	80	1
AHB19	Triethlyamine	10.75	1.0	13.36	3.97	170.79	44.07	173	—	—	1612	47[b]	1
AHB20	4-(Dimethylamino)-pyr.	9.60	1.0	17.42	4.06	171.02	44.15	173			1583	75	1

[a] n.d. – not determined. [b] Widths of bands of ^{13}C isotopologs of **AHB03** and **AHB19** were 49 and 60 cm^{-1}, while isotope shifts were 38 and 34 cm^{-1} respectively. In other cases, equal isotope shifts of 35 cm^{-1} were assumed in the fitting procedure of difference spectra.

of its complexes are likely not directly comparable to those of pyridines (just like aliphatic alcohols need a different treatment than phenols;[83] this is probably connected to the deshielding effects of the π-electron systems in phenols and pyridines). Secondly, the conclusions on proton donating/accepting abilities of species in aprotic media based on pK_a values obtained in water can only be reliable by comparison within a given class of compounds.[15] We note that a similar outlying of the data point was previously reported for the ν(OD) stretching frequency of methanol complexes with pyridines and aliphatic amines.[81]

3.2. FTIR spectra

It quickly became obvious during our initial attempts at correlating frequencies of vibrational modes of the carboxylic group of **AHB** complexes to the degree of proton transfer that while the ν(C═O) bands seemed to display a rather clear monotonic downshift between **AHB01** and **AHB10** (see full set of IR spectra in ESI,† Fig. S4–S10), corresponding spectral contributions become very broad and increasingly obscured by other transitions in later stages of the proton transfer making a quantitative analysis rather difficult. Conversely, $\nu_{as}(CO_2^-)$ may quite readily be assigned in case of **AHB19** only and is broad and obscured in other zwitterionic species. Similar problems as those just described for the 1800 to 1600 cm^{-1} spectral region preclude straightforward analysis of the region between 1400 and 1350 cm^{-1} region where ν(C–O) and $\nu_{sym}(CO_2^-)$ are located.[82]

In order to overcome this difficulty in this work we have conducted a combined FTIR study of acid–base complexes **AHB** both in natural isotope abundance and of their 1-^{13}C isotopologs of the chloroacetic acid moieties. The analysis of isotope difference spectra in which all spectral contributions unrelated to the carboxylic group should cancel was performed revealing the desired spectral information. A subset of corresponding data is shown in Fig. 5 in which orange and green traces correspond to systems containing chloroacetic acid in natural isotope abundance and 99% 1-^{13}C-labelled, respectively. Black solid traces are difference spectra (the spectrum of ^{13}C-labelled species minus the spectrum of non-labelled species, *i.e.* the green trace minus the orange trace).

The spectra of **AHB03** and **AHB19** (Fig. 5a) are most readily analyzed. Major features of the difference spectra of these species are dispersion shaped and centered on about 1710 and 1590 cm^{-1}, respectively. These major features in both cases may be fitted employing pairs of positive and negative Lorentzian peaks (sums represented by dotted lines). In case of **AHB03**, these peaks, corresponding to $\nu(^{12}C{=}O)$ and $\nu(^{13}C{=}O)$ are located at 1725 and 1687 cm^{-1} and have widths (FWHM) of 38 and 49 cm^{-1}, respectively. The frequencies and integrated intensities of the peaks are represented by the blue vertical bars. We note that there are several sharp features in the region of 1570 cm^{-1} (probably these are the ring mode vibrations of the pyridine moiety) that do not seem to be entirely indifferent to isotope substitution and hence do not entirely cancel in the difference spectrum. For **AHB19**, we attribute the peaks in the difference spectrum at 1612 and 1578 cm^{-1} (widths 47 and 60 cm^{-1}) to $\nu_{as}(^{12}CO_2^-)$ and $\nu_{as}(^{13}CO_2^-)$, respectively, represented by red vertical bars. We note that the isotope effects on vibrational frequencies in **AHB03** and **AHB19** are quite similar: 38 and 34 cm^{-1}, respectively.

The spectra of **AHB20** can be treated in analogy to the previous if care is taken to compensate in the fitting procedure for an additional sharp and somewhat intense dispersion shaped feature (two Lorentzian peaks of inverse sign, widths 15 cm^{-1}, offset 4 cm^{-1}) centered on 1550 cm^{-1} (the origin of this spectral feature is not clear). The dashed line in the figure represents the broad contribution only, attributable to $\tilde{\nu}_{as}(CO_2^-)$.

Lets us next address the spectrum of complex **AHB10** recorded at 178 K (Fig. 5b, bottom). The broad and complex shape of difference spectrum with maximum absolute values separated by as much as 100 cm^{-1} can hardly be treated in analogy to the previous spectra. Especially the suggestive double maximum structure of the spectrum of the ^{13}C isotopologue prompted us to try a dual band deconvolution approach on it, namely assuming coexistence of ν(C═O) and $\nu_{as}(CO_2^-)$ modes. Fitting the difference spectrum consequently involves four Lorentzian peaks, two per isotope. In order to assure numerical stability of the fitting algorithm, we fixed the isotope splitting in both modes to 35 cm^{-1} and constrained widths and areas of spectral contributions of each given mode to be identical by absolute values for both isotopologues. The total four Lorentzian fit functions are represented in Fig. 5 by black dashed lines. We observe that this approach well describes the data, especially when applied to spectra of **AHB10** acquired at temperatures higher than 178 K (upper part of Fig. 5b). The same procedure was employed successfully on the spectra of **AHB07** and **AHB14** at 173–178 K (Fig. 5a) and a number of other systems at various temperatures.

Summarizing the results in Fig. 5a we observe two concurrent monotonous trends within the series of spectra: firstly, band intensity is redistributed from ν(C═O) band (blue) to $\nu_{as}(CO_2^-)$ band (red), and, secondly, both bands, if present, shift to lower frequencies (red shift). Similar effects can be seen in temperature-dependent spectra for a given system, such as **AHB10**, shown in Fig. 5b: upon lowering the temperature the band intensity is redistributed from ν(C═O) band to $\nu_{as}(CO_2^-)$ band, and both bands shift to lower frequencies. The significance of these findings will be further elucidated in the Discussion.

3.3. *Ab initio* molecular dynamics simulations

While the detailed description of the results of *ab initio* MD simulations will be given in the next section, here we present the general information which will facilitate future discussion. For the complex of chloroacetic acid with 2-methylpyridine (complex **AHB10**) solvated by 71 CD_2Cl_2 molecules the trajectory (last 26 ps of it, 1 fs steps) was analyzed as described in Experimental section. A typical structure of the hydrogen bonded complex is shown in Fig. 7. The solvent molecules were removed from Fig. 7 for clarity.

To examine the geometry of the H-bond of the complex we have built distributions of its key geometric parameters along the trajectory, shown in Fig. 8. In each case in Fig. 8 it is depicted which angle or dihedral angle is being plotted. The plots in Fig. 8

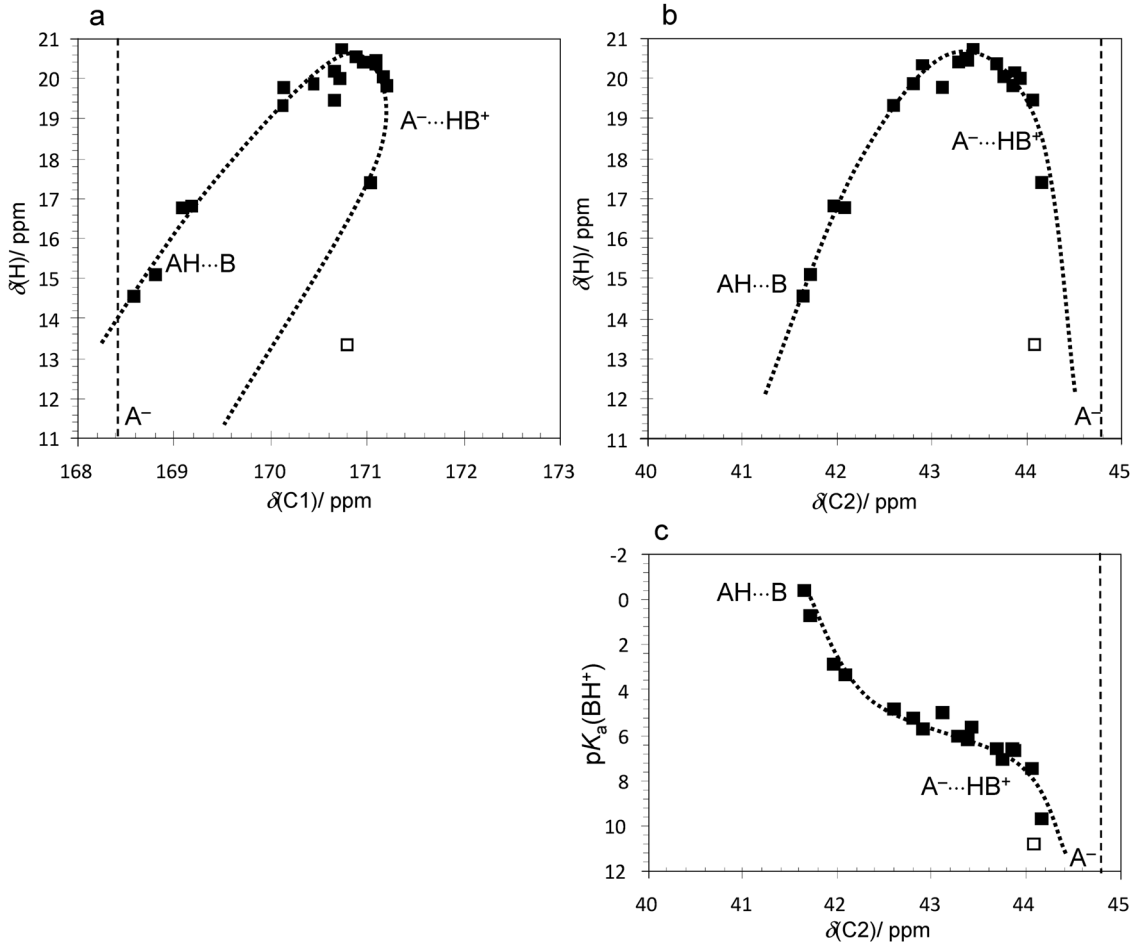

Fig. 6 Plots of NMR parameters of complexes **AHB01**–**AHB20** listed in Table 1. (a) δ(H) *vs.* δ(C1). (b) δ(H) *vs.* δ(C2). (c) pK_a(BH$^+$) *vs.* δ(C2). Open square point: **AHB19** (triethylamine complex). Vertical dashed line corresponds to the chloroacetic acid anion (**A**$^-$).

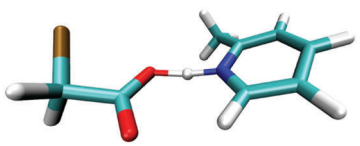

Fig. 7 The typical conformation of the **AHB10** complex according to the *ab initio* MD simulations. The solvent molecules are removed from the figure for clarity.

have been individually normalized so that abscissa numbers are not directly comparable.

During the whole course of the simulation the complex is not broken and the H-bond stays close to linear (Fig. 8a). *trans*-Configuration with respect to the mutual orientation of the "free" carbonyl group of the acid and methyl group of pyridine dominates (Fig. 8b), though there is a small peak in dihedral angle distribution at $\sim 60^\circ$ which indicates that *cis*-configuration is also present. Though the planar configuration is most probable, most of the time the instant conformation is non-planar. The H-bond of the complex is oriented along the lone pair of the nitrogen atom (Fig. 8c) and perpendicular to the line connecting two oxygen atoms of chloroacetic acid (Fig. 8d). The position of the bridging proton in the hydrogen bond changes significantly during the simulation. In Fig. 9 we show the time dependence of the proton position measured as the linear combination of interatomic distances $q_1 = 1/2\ (r_{OH} - r_{HN})$. The proton crosses the hydrogen bond center several times, effectively interconverting molecular O–H···N ($q_1 < 0$), and zwitterionic O$^-$···H–N$^+$ ($q_1 > 0$) structures.

4. Discussion

4.1. NMR spectra

While the chemical shift of the bridging proton certainly is one of the most prominent NMR parameters in the characterization of hydrogen bonds, its employment suffers from some drawbacks. One of these drawbacks, encountered particularly in studies of short hydrogen bonds, is that proton chemical shift passes a maximum when bridging proton crosses the H-bond center[83] and as a result it is sometimes hard to determine on which side of the H-bond center the proton resides. Several NMR parameters have been considered and employed to help to answer this question. For complexes of pyridines, the chemical

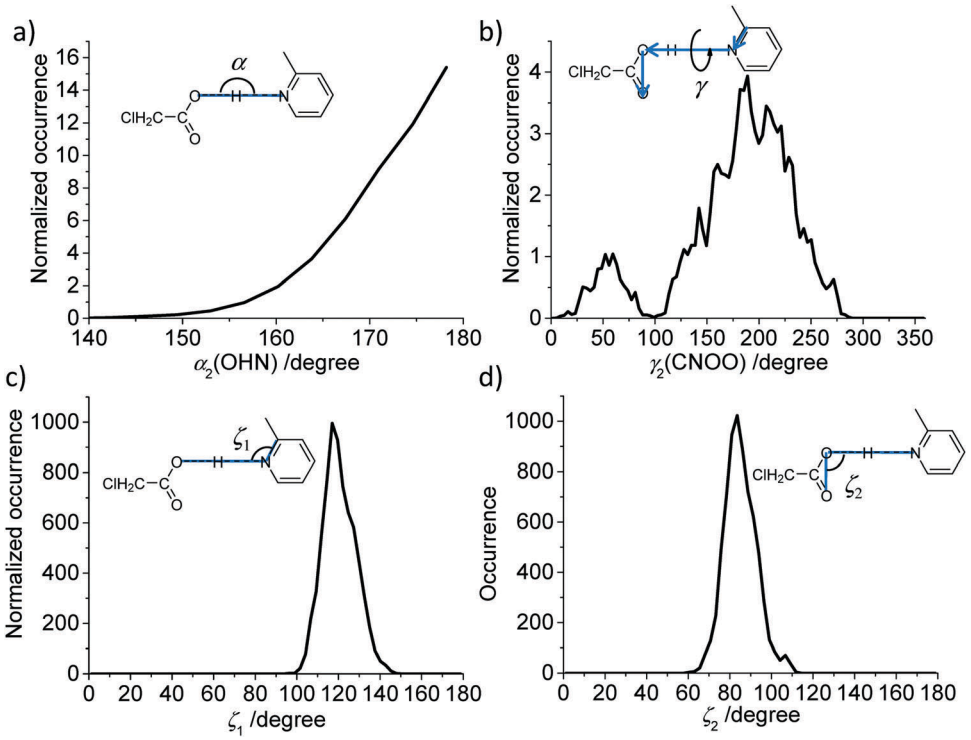

Fig. 8 The key geometrical parameters (exact definitions are given graphically for each plot) of the **AHB10** complex along the *ab initio* MD trajectory. (a) The OHN angle α which describes the linearity of the hydrogen bond; (b) the CNOO dihedral angle γ which describes the co-planarity of the pyridine ring and the COO group; (c) the CNO angle ζ_1 which describes how well the lone pair of the nitrogen atom points towards the oxygen atom involved in the hydrogen bond; (d) the NOO angle ζ_2 which describes the mutual orientation of the COO and pyridine moieties.

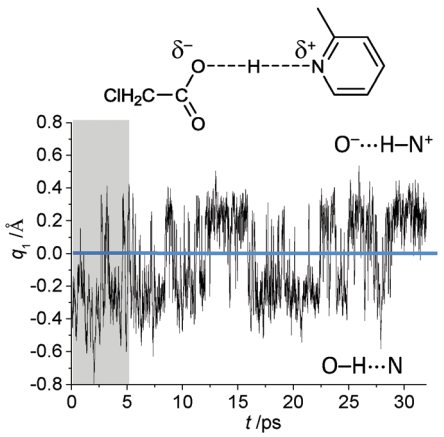

Fig. 9 Time evolution of the bridging proton position in the complex of chloroacetic acid with 2-methylpyridine (**AHB10**) according to *ab initio* MD simulation. Proton position is measured as $q_1 = 1/2(r_{OH} - r_{HN})$.

shift of ^{15}N,[35] H/D isotope effect on it,[29] $^1J_{NH}$ coupling constant[18b] and N–H dipole–dipole coupling[9] have been previously used. The sign of the primary H/D isotope effect has been proposed as a criterion to distinguish between symmetric and asymmetric proton positions in the bridge.[16] For hydrogen bonded complexes involving carboxylic acids, the chemical shift of carboxylic carbon δ(C1) and secondary H/D isotope effects on that parameter have been exploited with some success.[31,84]

Here, on the example of **AHB01**–**AHB20** complexes we show that δ(C2) correlates well with the bridging proton chemical shift δ(H) (Fig. 6b) and also it correlates in a sigmoidal fashion with pK_a(**BH**$^+$) of the base (Fig. 6c). We conclude that δ(C2) is a valuable parameter in the characterization of hydrogen bonds of this carboxylic acid. Despite the rather remote location of the C2 nucleus with respect to the hydrogen bond, δ(C2) offers a monotonous correlation to the degree of proton transfer and in this respect may be regarded superior to δ(C1). This means that the dotted curve in Fig. 6b represents in a way the proton transfer pathway (*i.e.* along this curve the proton transfer coordinate changes monotonously). The δ(H) *vs.* δ(C2) correlation can be affected – and is indeed affected, as will become clear after analyzing IR spectra – by the presence of the tautomeric equilibria between molecular and zwitterionic forms of the complexes. Similar effect has been previously observed for $\delta(^{15}N)$ *vs.* δ(H) correlation for pyridine–acid complexes and it is sometimes referred to as "corner-cutting effect",[85] which means that bridging proton chemical shift does not reach its maximal possible value.

4.2. FTIR spectra

The primary analysis of the isotope difference IR spectra performed as described in the Results section led to the set of ν(C=O) and $\nu_{as}(CO_2^-)$ band positions and corresponding relative integrated intensities for **AHB01**–**AHB20** complexes. In other words, the dual band structure in the IR spectra was

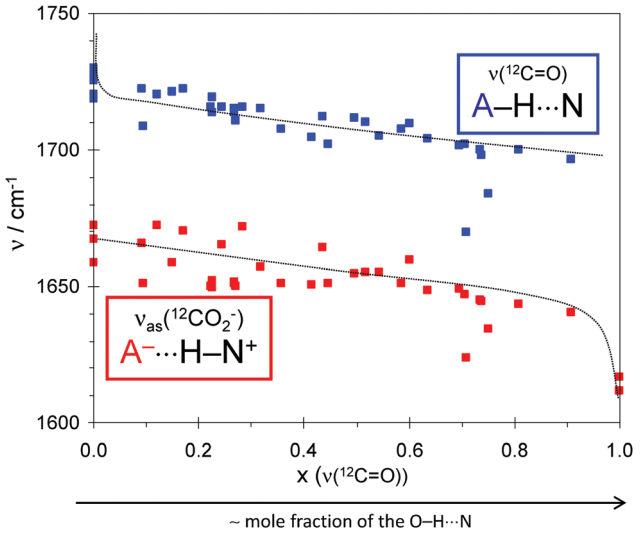

Fig. 10 The corresponding data points can be found in Table 1 and Table S1 (ESI†). The value x is the relative intensity of $\nu(^{12}C{=}O)$ band defined as $x = I\{\nu(^{12}C{=}O)\}/(I\{\nu(^{12}C{=}O)\} + I\{\nu_{as}(^{12}CO_2^-)\})$, where I stands for the integrated intensity of the corresponding IR band.

taken as a direct evidence of co-existence of proton tautomers: a molecular one O–H···N (giving rise to ν(C=O) band) and a zwitterionic one $O^-\cdots H{-}N^+$ (giving rise to $\nu_{as}(CO_2^-)$ band). As it was pointed out in Introduction, the two-state approach is an approximation, which does not take into account the variety of possible solvent shell configurations. We will come back to this when discussing the results of the *ab initio* MD simulation, but for the analysis of the IR spectra the two-state approximation works quite well. It was also mentioned in the Results section that with increased basicity of the base the IR band intensity is redistributed from ν(C=O) band to $\nu_{as}(CO_2^-)$ band and both bands shift to lower frequencies. This is visualized in Fig. 10 where we show $\nu(^{12}C{=}O)$ and $\nu_{as}(^{12}CO_2^-)$ band positions as a function of the relative intensity x of $\nu(^{12}C{=}O)$ band. In other words, x is defined as $I\{\nu(^{12}C{=}O)\}/(I\{\nu(^{12}C{=}O)\} + I\{\nu_{as}(^{12}CO_2^-)\})$, where I stands for the integrated intensity of the corresponding IR band. Thus, the band position might be considered as a "spectroscopic proton transfer coordinate", while the band intensities are proportional to the mole fractions of tautomers. We conclude that the combined proton transfer pathway similar to the one shown in Fig. 1c (and found previously for OHO^- hydrogen-bonded complexes[24]) applies here for OHN-bonded complexes **AHB01**–**AHB20**. The two-state interpretation of IR spectra does not invalidate the interpretation of δ(C2) NMR parameter as another "spectroscopic proton transfer coordinate". Indeed, δ(C2) averaged over two tautomers corresponds to the fictitious "average geometry" of the complex but remains monotonously dependent on the degree of proton transfer.

It is important to point out that all temperature points (Table 1 and Table S1, ESI†) are included into the Fig. 10 and they fall reasonably well on the same correlation line. Lowering the temperature leads to predictable and monotonous changes in the geometries of individual tautomers (measured as band positions)

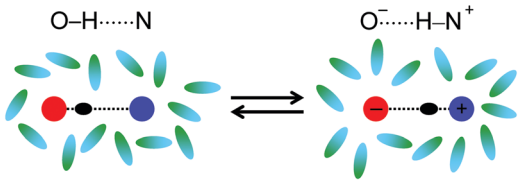

Fig. 11 Schematic representation of the solvent ordering (green-blue ovals) around molecular (left) and zwitterionic (right) forms of the OHN-bonded complex. The figure is aimed to illustrate purely "dielectric" way of describing solvent–solute interactions.

and their mole fractions (measured as relative band intensities). At this point, it is worth asking a question why the temperature affects the geometry of the complex at all? As one can safely neglect tiny changes in the populations of vibrational levels, the only remaining option is to consider the solvent–solute interactions. In our view, changes in the temperature lead to changes in the populations of various "solvatomers" (conformers of the solvation shell and the complex itself). One can look at it in two different ways, which will be described below.

One way to look at solvent–solute interactions and to roughly predict which solvatomers will be populated and which solvatomers will be depopulated upon lowering the temperature is to consider the effective polarity of the solvation shell. At lower temperatures the structures with higher ordering of the polar solvent molecules around the complex and subsequently higher dipole moment of the complex (higher degree of proton transfer; more zwitterionic nature) should be preferred. In contrast, at higher temperatures a less ordered solvation shell is more probable from the entropy point of view and as a result molecular structures of the complex with lower dipole moment should be preferred. The polarity argument (which can also be called dielectric argument) is illustrated schematically in Fig. 11.

Above, we have avoided using the term "dielectric constant of the solvent" as it is a macroscopic parameter and it should not be applied to individual molecules. However, the dielectric constant of dichloromethane rises upon temperature decrease (from 9 at room temperature to *ca.* 16 close to the freezing point[86]) and technically the presence of more polarizable medium should also stabilize more polar structures. In the next section we will briefly return to this question when describing the results of DFT calculations.

Another way of looking at solvent–solute interactions is to consider specific interactions such as CH hydrogen bonding between the solvent and the solute. This will be also discussed in the next section.

4.3. *Ab initio* MD simulations

We return to the analysis of the *ab initio* MD trajectory. In Fig. 12a the correlation between two hydrogen bond coordinates, namely, $q_1 = 1/2(r_{OH} - r_{HN})$ and $q_2 = r_{OH} + r_{HN}$, is shown. This correlation has the typical parabolic shape, established previously by neutron diffraction for hydrogen bonds of various types.[33,34] The q_1 *vs.* q_2 correlation shows that the shorter is the

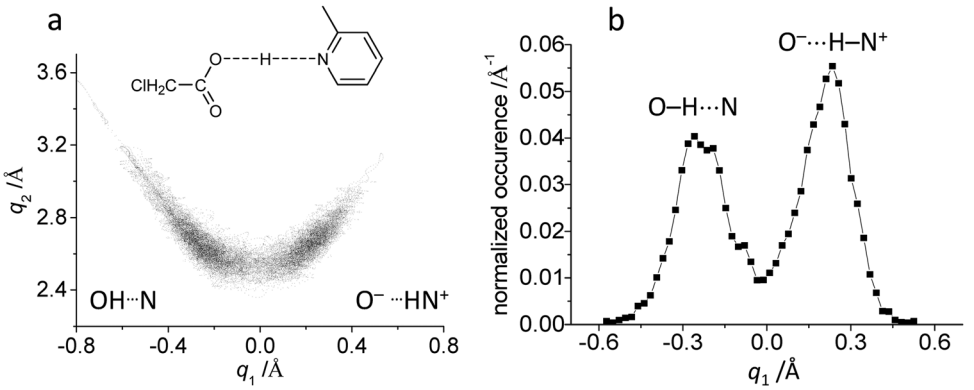

Fig. 12 Hydrogen bond geometries of **AHB10** complex, according to *ab initio* MD simulations. (a) Correlation between $q_1 = 1/2\,(r_{OH} - r_{HN})$ and $q_2 = r_{OH} + r_{HN}$ geometric parameters; (b) normalized occurence (having the meaning of the probability density) of q_1 values.

heavy atom distance, the closer is the bridging proton to the hydrogen bond center.

In Fig. 12a the density of points reflects the abundance of the structures in the simulation. Based on this, the proton position distribution (probability density or normalized occurence) has been constructed as a function of q_1 (Fig. 12b). This distribution has two broad but clearly visible maxima, which can be associated with O–H···N ($q_1 < 0$) and $O^-\cdots H\text{–}N^+$ ($q_1 > 0$) tautomers. The width of two peaks in Fig. 12b reflects the variety of solvatomers (and corresponding H-bond geometries) which all can be grouped into one or another "tautomer". There is also some probability density of finding the bridging proton very close to the middle of the hydrogen bond; such structures cannot be unambiguously assigned to either tautomer. Still, the relatively good separation of two maxima in Fig. 12b justifies the two-state approach used in the analysis of IR spectra. Less pronounced dual maximum proton distribution (and thus less clear case of two-state tautomerism) has been previously found by *ab initio* MD for $(OHO)^-$ hydrogen bonded complex of acetic acid with 4-nitrophenolate.[24]

In order to describe the kinetics of proton tautomerism one has to define first what constitutes the "jump" event. The first obvious requirement is that the sign of q_1 should change. However, one should also account for possible fast oscillations around q_1 = 0 Å which have more to do with the proton stretching vibration than with the proton tautomerism. In order to filter out such fluctuations we have included a second requirement: before and after the jump the system has to spend a certain time τ without changing the sign of q_1. In this way the number of jump events depends on τ. It seems physically reasonable to set τ to at least the duration of two or three proton stretching vibrational periods (*ca.* 20 fs each; keep in mind that in simulation all protons were treated as deutrons). In this approach for τ = 40 fs we obtain the average residence times of O–H···N and $O^-\cdots H\text{–}N^+$ tautomers equal to 0.62 ps and 0.76 ps, respectively, while the duration of the jump is about 20 fs. One of such jump events – a small section of the time dependence of Fig. 9 – is illustrated in Fig. 13.

The residence times obtained for other values of τ are given in Table S2 of ESI.† Taking into account the arbitrary nature of

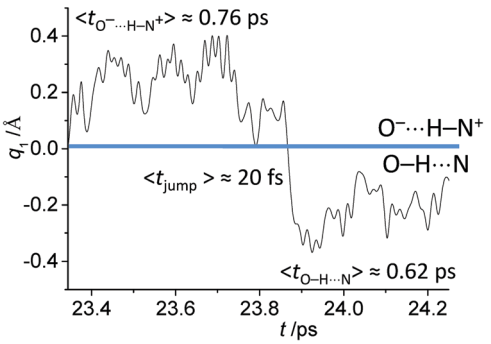

Fig. 13 Part of the *ab initio* MD trajectory for **AHB10** showing the jump of the bridging proton from $O^-\cdots H\text{–}N^+$ to O–H···N tautomers. The average residence times $\langle t_{O-H\cdots N}\rangle$ and $\langle t_{O^-\cdots H-N^+}\rangle$ are estimated for τ = 40 fs (for more details see text).

the definition of the jump event, it is advisable to take the exact values of the residence times with caution. However, in general the lifetimes of tautomers of about a picosecond seem to be reliable enough. For comparison, in Fig. S11 (ESI†) we plot the time dependence of q_1 where each point is averaged over 1 ps (so called window average; another way of filtering high-frequency noise), which gives us nine "jumps" for the whole trajectory. Interestingly, the estimated kinetics of proton tautomerism roughly matches the rotational diffusion times of dichloromethane, which is also in the order of a picosecond.[87,88]

The value of the residence time of a tautomer has an implication for the interpretation of the experimental IR spectra. To assess the magnitude of inhomogeneity and the impact of solvent fluctuations on spectral diffusion, ultrafast 2D-IR experiments appear to be the method of choice to elucidate the characteristic time scales, which we anticipate to have major components in the (sub)picosecond time range. In addition to that, the rapid jump of the bridging proton between the two sites as indicated by the *ab initio* trajectory of Fig. 13 suggests a dominant role of this exchange mechanism on similar time scales. In Fig. 14 we show power spectrum of **AHB10** in the region around 1600 cm^{-1} calculated from *ab initio* MD trajectory. Normal mode analysis[89] reveals that the selected region of the power spectrum contains only ν(C═O) and $\nu_{as}(CO_2^-)$ vibrations.

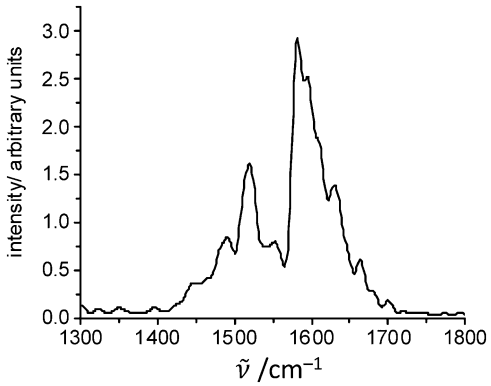

Fig. 14 Part of the power spectrum constructed from the *ab initio* MD trajectory for **AHB10** in the region of ν(C═O) and $\nu_{as}(CO_2^-)$ vibrations.

One can see that the dual-band shape of the power spectrum is consistent with the existence of two tautomers and also with the dual-band feature of experimental IR spectra (though one should not compare the intensities).

Now we come to the question of the direct causes of the proton jumps. As it was mentioned above, there are different possible scenarios here, which we discuss in the following paragraphs.

Firstly, the solvent ordering might create electric fields in the region of the OHN hydrogen bond, which displace the light bridging particle due to its high atomic polarizability (because of the shallow proton stretching potential in the short strong H-bond). This in turn increases the dipole moment of the solute by proton transfer from molecular to zwitterionic form. By analyzing the *ab initio* MD trajectory and assigning point atomic charges to all atoms of the solvent molecules, we have constructed the distribution of electrostatic field components due to the solvent molecules. The electrostatic field was projected along the ON axis for two points in space: at the bridging proton position (Fig. 15a) and at the geometric center between O and N atoms (Fig. 15b), as a function of q_1. It seems that the overall electric field situation is almost identical for molecular ($q_1 < 0$) and zwitterionic ($q_1 > 0$) tautomers. This is remarkable, because in principle one could have expected strong electrostatic field effects in a system that can significantly change its dipole moment by proton transfer.

Another way to evaluate the electrostatic interactions between the solvent molecules and the solvated complex is to construct a parameter describing how well solvent molecules orient their individual dipole moments along the electrostatic field created by the dipole moment of the solvated complex. Following this logic, for each time step of the sampling and for all solvent molecules we have calculated the order parameter λ defined as shown in the top part of Fig. 16 (to construct the dipole moment of the complex we have assigned the charge plus one to the nitrogen atom and minus one to the oxygen atom of the OHN bridge). The correlation between λ and q_1 is shown in the bottom part of Fig. 16. The order parameter seems to be close to zero on average and one can barely discern an asymmetry in the correlation, indicating that there is no dipole–dipole solvent ordering in the solvation box as a whole.

Yet another way to treat the effect of the electrostatic field is to model the solvent as the polarizable continuum. We have performed additional DFT calculations (B3LYP/6-311++G(d,p), PCM, other details see in ESI†) of the equilibrium structures and of the potential energy curves along the proton transfer coordinate for **AHB10** at various values of the dielectric constant of the medium ε. The results are presented in Fig. S12 (ESI†). In short, these calculations show that in vacuum the only existing energy minimum corresponds to the O–H···N structure, while upon ε increase the second minimum develops, corresponding to the $O^-\cdots H\text{–}N^+$ structure. However, at $\varepsilon = 20$ the energy barrier between two minima is only 1 kcal mole^{-1}, which is too low to consider individual tautomers (the zero-point vibrational level should lie higher than the top of the barrier). Interestingly enough, not the development of the second minimum but rather a smooth "mesomeric" proton transfer was previously experimentally found for Cl–H···NH_3

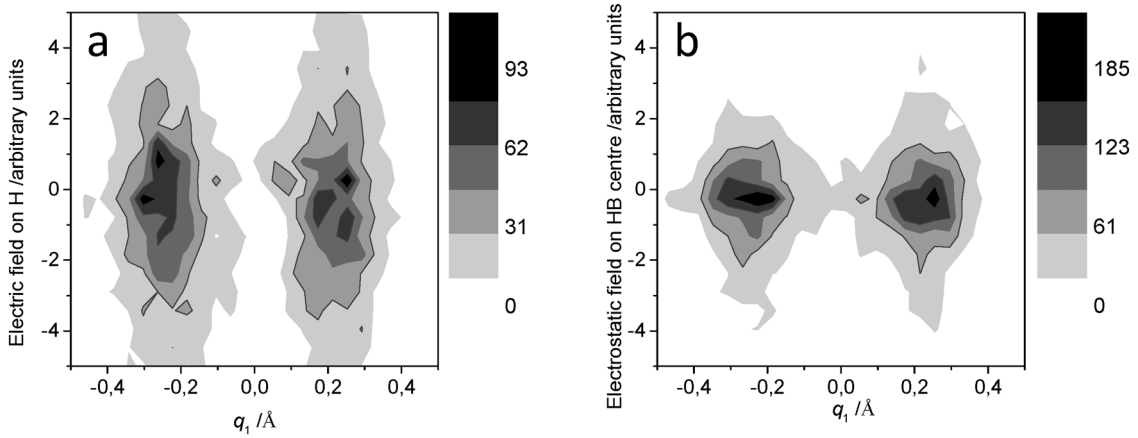

Fig. 15 Distribution of electrostatic field component along the ON axis due to solvent molecules approximated by point charges. Distribution is constructed for two points in space: at the bridging proton position (a) and at the geometric center between O and N atoms (b), as a function of q_1. The gray-scales are given in the number of counts.

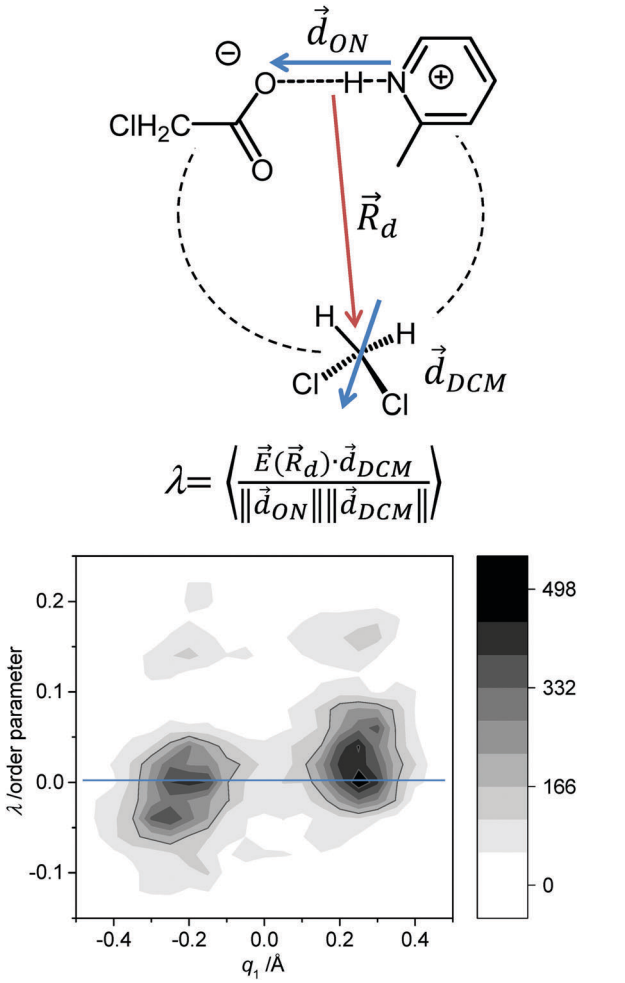

Fig. 16 The definition of the order parameter λ and the correlation between λ and q_1 constructed for all solvent molecules in the simulation box. The gray-scale is given in the number of counts.

complexes in noble gas matrices with increasing polarizability of matrix atoms.[19,20] There are also some experimental indications that the "dielectric argument" does not describe the situation sufficiently. Additional NMR experiments (not shown) revealed that addition of a few percent of chloroform to dichloromethane samples of chloroacetic acid pyridine complexes lead to an increase of proton transfer towards the base for given temperatures. This phenomenon is hard to rationalize in terms of the dielectric continuum model: the dielectric constant of chloroform is roughly half that of dichloromethane[90] and the decrease in solvent polarity by chloroform addition should lead to a decrease in proton transfer (see *e.g.* ref. 29). However, the above observation one can understand considering solvent solute hydrogen bonding, which is discussed in the next paragraph. Such hydrogen bonding is expected to be stronger in case of chloroform, which is a stronger proton donor than dichloromethane; the significance of this will become apparent below.

Let us now consider the influence that specific interactions, such as weak CHO hydrogen bonds between the solute and the solvent, might have on the geometry of the strong hydrogen bond in the solute complex. Previously, such H-bonds have been found for the anionic complex of acetic acid with nitrophenolate in CD_2Cl_2.[24] At this point we should mention that in limiting cases some of specific solvent solute interactions might be qualified as electrostatic interactions rather than weak H-bonds. However, in this work we omit such distinction and refer to all specific CHO solvent-interactions as to hydrogen bonds, as we believe it captured their essential characteristics. In this work we have tried a number of geometric parameters of the solvation shell and show the results only for those which give better correlations with the OHN bridging proton position. In Fig. 17 we plot the correlation between r_2 distance from the oxygen atom of "free" carbonyl to dichloromethane protons and CHO angle ϕ_2 for **AHB10**, subdivided into two parts: for $q_1 < 0$ (Fig. 17a) and $q_1 > 0$ (Fig. 17b). Only those snapshots of the trajectory were included in Fig. 17, in which the q_2 parameter (see Fig. 12) was shorter than 2.8 Å, as for the longer distances proton jumps become increasingly unlikely.

One can notice that for zwitterionic structures the solvent molecules form slightly stronger (shorter) CHO hydrogen bonds with the "free" carbonyl group. This suggests the cooperative coupling of CHO and OHN hydrogen bonds as a mechanism of proton transfer: strengthening of the CHO bond leads to a partial charge transfer and decreases the negative charge on the carboxylic group, which in turn decreases the proton accepting ability of the oxygen atom involved in the OHN bond. As a result the structure with the proton transfer is being preferentially stabilized.

A correlation similar to the one shown in Fig. 17 can be constructed for the r_1 distance from the oxygen atom of OHN bridge to dichloromethane protons and CHO angle ϕ_1 for **AHB10** (see Fig. 18). One can see that while the protons of the solvent molecules are generally further away, there is still a strengthening of the CHO hydrogen bond for zwitterionic structures.

In summary, the dielectric effects on the bridging proton position are likely to play a certain role, but the explicit calculations of the local electrostatic field of the solvent approximated by the point atomic charges along the *ab initio* MD trajectory did not reveal it. In other words, contrary to the common knowledge electric field fluctuations and dipole orientation – which is basically a PCM representation of the solvent – is only weakly correlated with the bridging proton position in the hydrogen bond. However all atom representation of the solvent is way more informative: specific solvent–solute interactions (breakage/formation of a weak hydrogen bond with the solvent) are well correlated with the OHN proton position. This is another indication that individual atoms and their positions matter a lot in a proper description of solvent solute interactions. The mechanism of proton transfer is illustrated in Fig. 19. One can also look at this in an opposite way: the proton position in the short strong OHN hydrogen bond appeared to be a sensitive indicator of the formation of weak CHO hydrogen bonds with the solvent.

In the final part of the analysis of the MD simulation we turn to the calculation of NMR parameters. For a randomly selected 98 snapshots from the trajectory we have calculated NMR chemical shifts (as described in Experimental section) for the

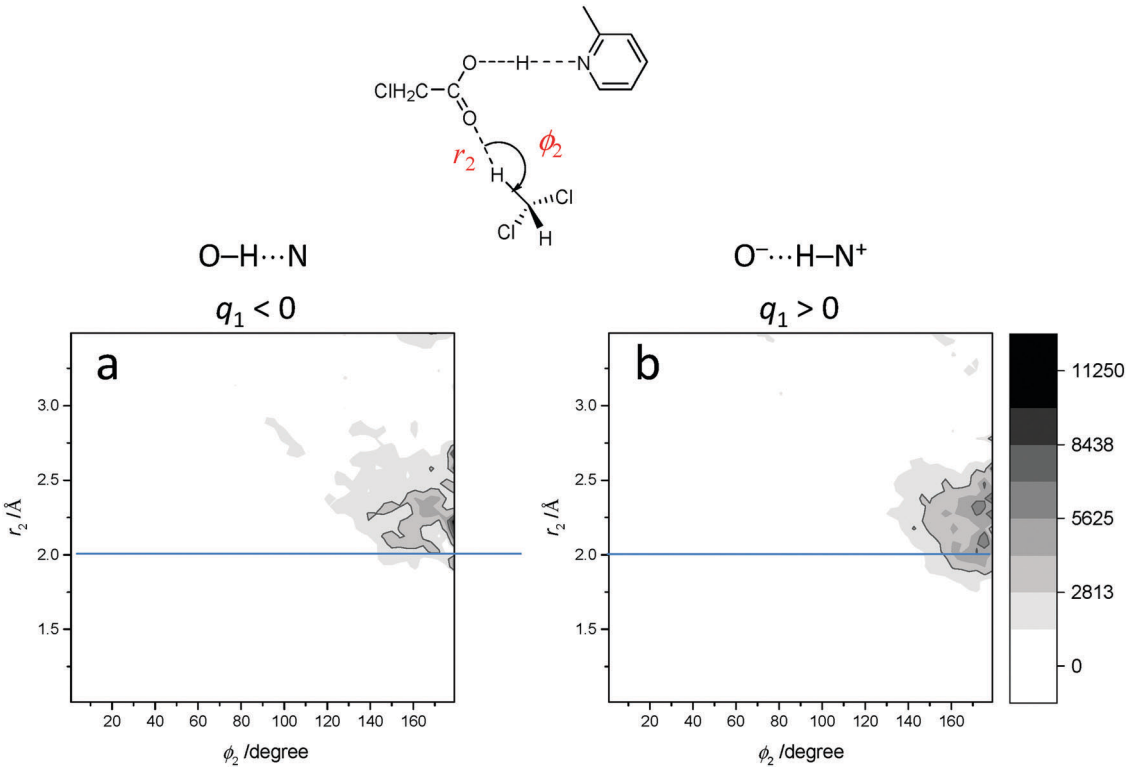

Fig. 17 Correlation between distance r_2 from the oxygen atom of "free" carbonyl to dichloromethane protons and CHO angle ϕ_2 for the *ab initio* MD trajectory for **AHB10** (with additional requirement $q_2 < 2.8$ Å) subdivided into two parts: for $q_1 < 0$ (a) and $q_1 > 0$ (b). Darker colours correspond to higher intensity (the scale in the right part of the figure corresponds to the occurrence, *i.e.* the number of counts).

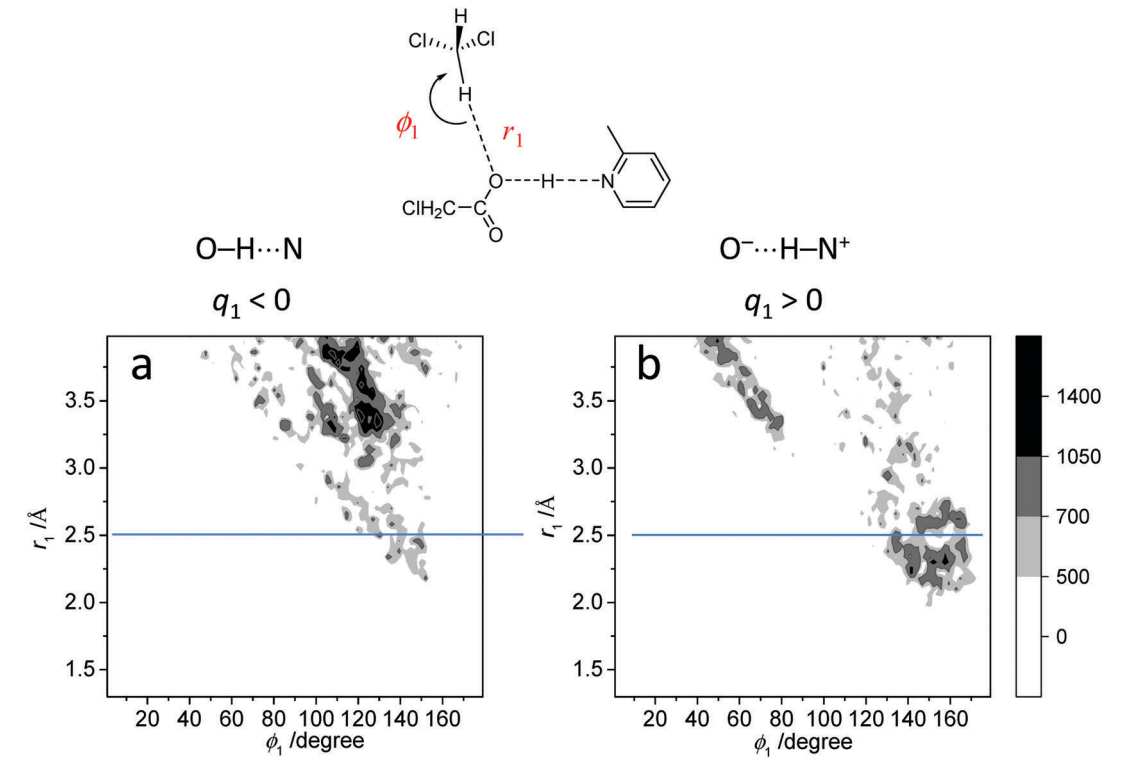

Fig. 18 Correlation between distance r_1 from the oxygen atom of OHN bridge to dichloromethane protons and CHO angle ϕ_1 for the *ab initio* MD trajectory for **AHB10** (with additional requirement $q_2 < 2.8$ Å) subdivided into two parts: for $q_1 < 0$ (a) and $q_1 > 0$ (b). Darker colours correspond to higher intensity (the scale in the right part of the figure corresponds to the occurrence, *i.e.* the number of counts).

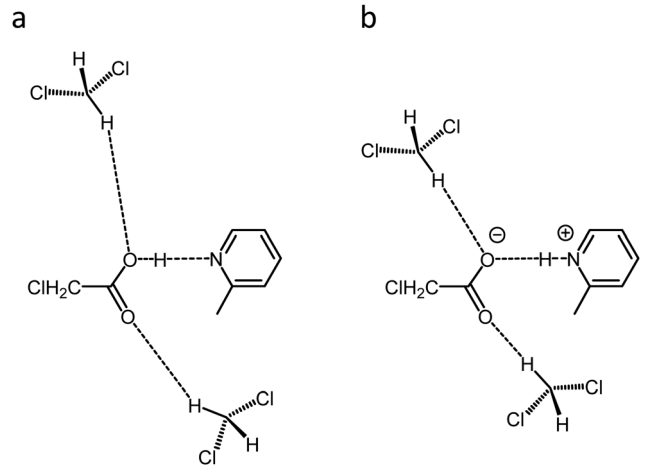

Fig. 19 Schematic representation of the O–H···N and $O^{-}\cdots H-N^{+}$ structures with relative positions of the solvent molecule nearest to "free" carbonyl group. (a) Molecular complex exhibiting weaker (longer) CHO hydrogen bonds with the nearest solvent molecules; (b) zwitterionic complex exhibiting stronger (shorter) CHO hydrogen bonds with the nearest solvent molecules.

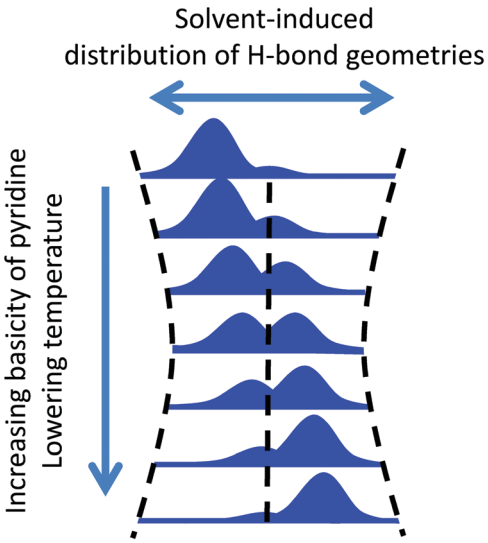

Fig. 21 Schematic representation of the overall proton transfer pathway for OHN-bonded complexes formed by chloroacetic acid with pyridines in solution in CD_2Cl_2.

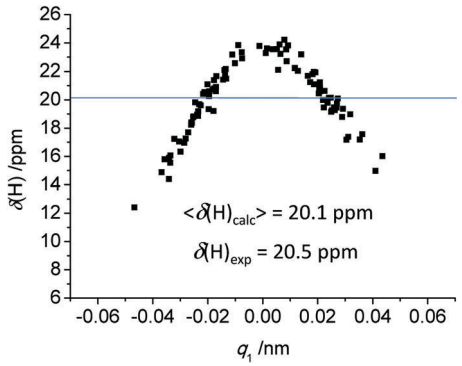

Fig. 20 Bridging proton chemical shift for **AHB10** complex, calculated for 98 random snapshots of the *ab initio* MD trajectory. The blue horizontal line corresponds to the average value. The experimental value of $\delta(H)_{exp}$, measured at 178 K, is also given.

bridging proton (Fig. 20), as well as C1, C2 carbons of chloroacetic acid and nitrogen nucleus of methylpyridine (Fig. S13, ESI†).

The proton chemical shift shows the expected parabolic behavior and the average calculated value $\langle\delta(H)_{calc}\rangle$ = 20.1 ppm fits surprisingly well to the experimental value $\delta(H)_{exp}$ = 20.5 ppm, which supports the notion that the computed trajectory represents the actual situation in the solution. The maximal value of proton chemical shift is *ca.* 24 ppm, probably due to the presence of ring currents in the pyridine ring moiety. Carbon chemical shifts are less informative, as they apparently depend on a number of variables (bond distances, angles, dihedral angles) apart of the dependence on the bridging proton position.[91] Averaging over these non-essential variables starts to reveal the dependence of the H-bond geometry (see Fig. S5, ESI†), despite the fact that the absolute values were not scaled and numerically they are off the experimental ones. Sampling more snapshots of the trajectory would increase the quality of the averaging. Finally, the nitrogen chemical shifts are less scattered and show the expected high-field shift of about 130 ppm upon protonation of pyridine (Fig. S5, ESI†).[9,29,85]

5. Conclusions

We have studied a series of intermolecular hydrogen-bonded 1 : 1 complexes formed by chloroacetic acid with 19 substituted pyridines and one aliphatic amine dissolved in CD_2Cl_2 at low temperature by ^{1}H, ^{13}C NMR and FTIR spectroscopy. The hydrogen bond geometries in these complexes vary from molecular (O–H···N) to zwitterionic ($O^{-}\cdots H-N^{+}$) ones. The NMR spectra showed formation of short strong H-bonds in intermediate cases. For the same complexes, analysis of C=O stretching and asymmetric CO_2^{-} stretching bands in FTIR spectra revealed presence of proton tautomerism. On the basis of these data, the overall proton transfer pathway was constructed, which is schematically shown in Fig. 21. For most of the complexes a dual-maximum distribution of hydrogen bond geometries exists in solution, and upon changing proton acceptor or temperature the positions of these two maxima change together with their relative intensities. Such proton transfer pathway is combining features of a classical "tautomeric" (Fig. 1a) and classical "mesomeric" (Fig. 1b) pathways.

The description given above is due to the solvent–solute interactions, both dielectric (dipole–dipole) and specific (weak H-bonding to the solvent). The distribution of hydrogen bond geometries in the ensemble of solvatomers and the properties of the solvation shell causing proton jumps have been investigated by *ab initio* MD simulations performed for one of the complexes, namely, a chloroacetic acid complex with 2-methylpyridine. We showed that the electric field fluctuations (PCM-like approach) is only weakly correlated with H-bond geometry. At the same time,

specific solvent–solute interactions such as strengthening/weakening of C–H···O=C hydrogen bonds between CD_2Cl_2 solvent molecules and oxygen atoms of the acid correlate with the bridging proton position in the strong OHN bond and it is likely to be one of the major causes for proton jumps (see Fig. 19). This illustrates how all atom representation of the solvent improves the overall description of the hydrogen bonded complexes in condensed phase.

Acknowledgements

NMR and IR measurements and were performed within the framework of a grant from the Deutsche Forschungsgemeinschaft (Project No. DFG – NI 492/11-1). *Ab initio* MD simulations were performed within the framework of a grant from the Deutsche Forschungsgemeinschaft Se1008/11-1. The analysis of the CHO hydrogen bonding with the solvent was performed within the framework of the RFBR grant 14-03-00111. The analysis of the OHN hydrogen bond geometry was performed within the framework of the RFBR grant 15-03-04605. We thank Dr Andrei Gurinov for the synthesis of 3-bromo-2,4,6-collidine. This work is supported by the travel grant (SP) by German-Russian Interdisciplinary Science Center (G-RISC) funded by the German Federal Foreign Office *via* the German Academic Exchange Service (DAAD).

References

1 C. L. Perrin, J. S. Lau and B. K. Ohta, Low-Barrier Hydrogen Bonds in Pyridine–Dichloroacetic Acid Complexes, *Pol. J. Chem.*, 2003, **77**, 1693–1703.

2 G. M. Barrow, The Nature of Hydrogen Bonded Ion-Pairs: The Reaction of Pyridine and Carboxylic Acids in Chloroform, *J. Am. Chem. Soc.*, 1956, **78**, 5802–5806.

3 G. S. Denisov, J. Starosta and V. M. Schreiber, Spectra of complexes with hydrogen bond and of ion pairs in the long-wavelength IR region (700–70 cm^{-1}). The system pyridine-acid, *Opt. Spektrosk.*, 1973, **35**, 447–452.

4 J. Nasielski and E. Vander Donckt, Propriétés physico-chimiques de composés à caractère aromatique—V: Etude, par spectroscopie ultraviolette, de l'interaction entre les dérivés monoazaaromatiques et les acides carboxyliques. Mise en évidence d'un potentiel à deux minimums pour le lien hydrogène, *Spectrochim. Acta*, 1963, **19**, 1989–2009.

5 T. Scharge, T. N. Wassermann and M. A. Suhm, Weak hydrogen bonds make a difference: Dimers of jet-cooled halogenated ethanols, *Z. Phys. Chem.*, 2008, **222**, 1407–1452.

6 L. O. Paulson and D. T. Anderson, High-Resolution Vibrational Spectroscopy of trans-Formic Acid in Solid Parahydrogen, *J. Phys. Chem. A*, 2009, **113**, 1770–1778.

7 T. Yamashita and K. Takatsuka, Hydrogen-bond assisted enormous broadening of infrared spectra of phenol-water cationic cluster: An ab initio mixed quantum-classical study, *J. Chem. Phys.*, 2007, **126**, 074304.

8 G. V. Gusakova, G. S. Denisov, A. L. Smolyansky and V. M. Schreiber, Hydrogen bond and proton transfer in carboxylic acid-amin system. Spectroscopic study of the equilibrium between the molecular complex and the ion pair, *Doklady Akad. Sci.*, 1970, **193**, 1065–1068.

9 N. S. Golubev, G. S. Denisov and A. I. Koltsov, Proton Spin-Spin Coupling in Complexes of Formic Acid with Proton Acceptors, *J. Mol. Struct.*, 1981, **75**, 333–337.

10 P. Lorente, I. G. Shenderovich, G. Buntkowsky, N. S. Golubev, G. S. Denisov and H. H. Limbach, $^{1}H/^{15}N$ NMR chemical shielding, dipolar $^{15}N,^{2}H$ coupling and hydrogen bond geometry correlations in a novel series of hydrogen bonded acid–base complexes of collidine with carboxylic acids, *Magn. Reson. Chem.*, 2001, **39**, S18–S29.

11 H.-H. Limbach, G. S. Denisov, I. G. Shenderovich and P. M. Tolstoy, ''Proton Tautomerism in Systems of Increasing Complexity: Examples from Organic Molecules to Enzymes'' in *Tautomerism: Concepts and Applications in Science and Technology*, ed. L. Antonov, Wiley-VCH Verlag GmbH & Co. KGaA, 2016, pp. 329–372.

12 Z. Dega-Szafran and E. Dulewicz, ^{1}H NMR Studies of Solvent Effects on Hydrogen Bonding in Some Pyridine Trifluoroacetates, *Org. Magn. Reson.*, 1981, **16**, 214–219.

13 N. S. Golubev, S. N. Smirnov, P. M. Tolstoy, S. Sharif, M. D. Toney, G. S. Denisov and H.-H. Limbach, Observation by NMR of the tautomerism of an intramolecular OHOHN-charge relay chain in a model Schiff base, *J. Mol. Struct.*, 2007, **844**, 319–327.

14 B. Koeppe, P. M. Tolstoy and H.-H. Limbach, Reaction Pathways of Proton Transfer in Hydrogen Bonded Phenol-Carboxylate Complexes Explored by UVNMR, *J. Am. Chem. Soc.*, 2011, **133**, 7897–7908.

15 B. Koeppe, J. Guo, P. M. Tolstoy, G. S. Denisov and H.-H. Limbach, Solvent and H/D Isotope Effects on the Proton Transfer Pathways in Heteroconjugated Hydrogen-Bonded Phenol-Carboxylic Acid Anions Observed by Combined UV–vis and NMR Spectroscopy, *J. Am. Chem. Soc.*, 2013, **135**, 7553–7566.

16 P. Schah-Mohammedi, I. G. Shenderovich, C. Detering, H.-H. Limbach, P. M. Tolstoy, S. N. Smirnov, G. S. Denisov and N. S. Golubev, Hydrogen/Deuterium Isotope Effects on NMR Chemical Shifts of Formally Symmetric Complexes with a Strong Intermolecular Hydrogen Bond in Liquid Solutions at 100–150 K, *J. Am. Chem. Soc.*, 2000, **122**, 12878–12879.

17 S. N. Smirnov, N. S. Golubev, G. S. Denisov, H. Benedict, P. Schah-Mohammedi and H. H. Limbach, Hydrogen/Deuterium Isotope Effects on the NMR Chemical Shifts and Geometries of Intermolecular Low-Barrier Hydrogen Bonded Complexes, *J. Am. Chem. Soc.*, 1996, **118**, 4094–4101.

18 (*a*) I. G. Shenderovich, H.-H. Limbach, S. N. Smirnov, P. M. Tolstoy, G. S. Denisov and N. S. Golubev, H/D Isotope Effects on the Low-temperature NMR Parameters and Hydrogen Bond Geometries of $(FH)_2F^-$ and $(FH)_3F^-$ dissolved in CDF_3/CDF_2Cl, *Phys. Chem. Chem. Phys.*, 2002, **4**, 5488–5497; (*b*) I. G. Shenderovich, P. M. Tolstoy, N. S. Golubev, S. N. Smirnov, G. S. Denisov and H.-H. Limbach, Low-temperature

NMR Studies of the Structure and Dynamics of a Novel Series of Acid–Base Complexes of HF with Collidine Exhibiting Scalar Couplings Across Hydrogen Bonds, *J. Am. Chem. Soc.*, 2003, **125**, 11710–11720.

19 A. J. Barnes and A. C. Legon, Proton transfer in amine-hydrogen halide complexes: comparison of low temperature matrices with the gas phase, *J. Mol. Struct.*, 1998, **448**, 101–106.

20 L. Andrews, X. Wang and Z. Mielke, Infrared Spectrum of the H_3N-HCl Complex in Solid Ne, Ne/Ar, Ar, and Kr. Matrix Effects on a Strong Hydrogen-Bonded Complex, *J. Phys. Chem. A*, 2001, **105**, 6054–6064.

21 S. Sharif, G. S. Denisov, M. D. Toney and H.-H. Limbach, NMR Studies of Coupled Low- and High-Barrier Hydrogen Bonds in Pyridoxal-5′-Phosphate Model Systems in Polar Solution, *J. Am. Chem. Soc.*, 2007, **129**, 6313–6327.

22 J. Guo, P. M. Tolstoy, B. Koeppe, N. S. Golubev, G. S. Denisov, S. N. Smirnov and H.-H. Limbach, Hydrogen Bond Geometries and Proton Tautomerism of Homo-Conjugated Anions of Carboxylic Acids Studied via H/D Isotope Effects on ^{13}C NMR Chemical Shifts, *J. Phys. Chem. A*, 2012, **116**, 11180–11188.

23 M. Garcia-Viloca, A. Gonzalez-Lafont and J. M. Lluch, Asymmetry of the Hydrogen Bond of Hydrogen Phthalate Anion in Solution. A QM/MM Study, *J. Am. Chem. Soc.*, 1999, **121**, 9198–9207.

24 S. Pylaeva, C. Allolio, B. Koeppe, G. S. Denisov, H.-H. Limbach, D. Sebastiani and P. M. Tolstoy, Proton transfer in a short hydrogen bond caused by solvation shell fluctuations: an ab initio MD and NMR/UV study of an $(OHO)^-$ bonded system, *Phys. Chem. Chem. Phys.*, 2015, **17**, 4634–4644.

25 Y. Mori and Y. Masuda, Effect of solvent on proton location and dynamic behavior in short intramolecular hydrogen bonds studied by molecular dynamics simulations and NMR experiments, *Chem. Phys.*, 2015, **458**, 18–29.

26 T. Steiner, I. Majerz and C. C. Wilson, First O–H–N Hydrogen Bond with a Centered Proton Obtained by Thermally Induced Proton Migration, *Angew. Chem., Int. Ed.*, 2001, **40**, 2651–2654.

27 T. Steiner, C. C. Wilson and I. Majerz, Neutron diffraction study of a very short O–H···N hydrogen bond: crystalline adduct of 2-methylpyridine and pentachlorophenol, *Chem. Commun.*, 2000, 1231–1232.

28 S. N. Smirnov, H. Benedict, N. S. Golubev, G. S. Denisov, M. M. Kreevoy, R. L. Schowen and H. H. Limbach, Exploring Zero-point Energies and Hydrogen Bond Geometries along Proton Transfer Pathways by Low-temperature NMR, *Can. J. Chem.*, 1999, **77**, 943–949.

29 P. M. Tolstoy, S. N. Smirnov, I. G. Shenderovich, N. S. Golubev, G. S. Denisov and H. H. Limbach, NMR Studies of Solid State - Solvent and H/D Isotope Effects on Hydrogen Bond Geometries of 1:1 Complexes of Collidine with Carboxylic Acids, *J. Mol. Struct.*, 2004, **700**, 19–27.

30 H. H. Limbach, M. Pietrzak, S. Sharif, P. M. Tolstoy, I. G. Shenderovich, S. N. Smirnov, N. S. Golubev and G. S. Denisov, NMR-Parameters and Geometries of OHN and ODN Hydrogen Bonds of Pyridine–Acid Complexes, *Chem. – Eur. J.*, 2004, **10**, 5195–5204.

31 P. M. Tolstoy, J. Guo, B. Koeppe, N. S. Golubev, G. S. Denisov, S. N. Smirnov and H. H. Limbach, Geometries and Tautomerism of OHN Hydrogen Bonds in Polar Solution probed by H/D Isotope Effects on ^{13}C NMR Chemical Shifts, *J. Phys. Chem. A*, 2010, **114**, 10775–10782.

32 B. C. K. Ip, I. G. Shenderovich, P. M. Tolstoy, J. Frydel, G. S. Denisov, G. Buntkowsky and H. H. Limbach, NMR Studies of Solid Pentachlorophenol-4-Methylpyridine Complexes Exhibiting Strong OHN Hydrogen Bonds: Geometric H/D Isotope Effects and Hydrogen Bond Coupling Cause Isotopic Polymorphism, *J. Phys. Chem. A*, 2012, **116**, 11370–11387.

33 T. J. Steiner and W. Saenger, Lengthening of the covalent O–H bond in O–H···O hydrogen bonds re-examined from low-temperature neutron diffraction data of organic compounds, *Acta Crystallogr., Sect. B: Struct. Sci.*, 1994, **50**, 348–357.

34 T. Steiner, Lengthening of the Covalent X–H Bond in Heteronuclear Hydrogen Bonds Quantified from Organic and Organometallic Neutron Crystal Structures, *J. Phys. Chem. A*, 1998, **102**, 7041–7052.

35 S. Sharif, E. Fogle, M. D. Toney, G. S. Denisov, I. G. Shenderovich, G. Buntkowsky, P. M. Tolstoy, M. Chan Huot and H. H. Limbach, NMR Localization of Protons in Critical Enzyme Hydrogen Bonds, *J. Am. Chem. Soc.*, 2007, **129**, 9558–9559.

36 G. S. Denisov and V. M. Schreiber, Infrared Study of the Interaction of Pentachlorophenol with Secondary Amines, *Spectrosc. Lett.*, 1972, **5**, 377–384.

37 G. S. Denisov and V. M. Schreiber, The Evolution of the Potential Surface of Chlorophenoles – Amines Interaction, *Doklady Akad. Sci.*, 1974, **215**, 310–313.

38 E. Libowitzki, Correlation of O–H Stretching Frequencies and O–H···O Hydrogen Bond Lengths in Minerals, *Monatsh. Chem.*, 1999, **130**, 1047–1059.

39 J. Emsley, Very strong hydrogen bonding, *Chem. Soc. Rev.*, 1980, **9**, 91–124.

40 W. Mikenda, Stretching frequency versus bond distance correlation of O–D(H)···Y (Y = N, O, S, Se, Cl, Br, I) hydrogen bonds in solid hydrates, *J. Mol. Struct.*, 1986, **147**, 1–15.

41 A. Novak, Hydrogen bonding in solids correlation of spectroscopic and crystallographic data, *Struct. Bonding*, 1974, **18**, 177–216.

42 A. Lautié, F. Froment and A. Novak, Relationship between NH Stretching Frequencies and N···O Distances of Crystals Containing NH···O Hydrogen-Bonds, *Spectrosc. Lett.*, 1976, **9**, 289–299.

43 E. T. J. Nibbering and T. Elsaesser, Ultrafast vibrational dynamics of hydrogen bonds in the condensed phase, *Chem. Rev.*, 2004, **104**, 1887–1914.

44 C. J. Fecko, J. D. Eaves, J. J. Loparo, A. Tokmakoff and P. L. Geissler, Ultrafast hydrogen-bond dynamics in the infrared spectroscopy of water, *Science*, 2003, **301**, 1698–1702.

45 J. B. Asbury, T. Steinel, C. Stromberg, S. A. Corcelli, C. P. Lawrence, J. L. Skinner and M. D. Fayer, Water dynamics: Vibrational echo correlation spectroscopy and comparison to molecular dynamics simulations, *J. Phys. Chem. A*, 2004, **108**, 1107–1119.

46 M. L. Cowan, B. D. Bruner, N. Huse, J. R. Dwyer, B. Chugh, E. T. J. Nibbering, T. Elsaesser and R. J. D. Miller, Ultrafast memory loss and energy redistribution in the hydrogen bond network of liquid H_2O, *Nature*, 2005, **434**, 199–202.
47 D. Laage and J. T. Hynes, A molecular jump mechanism of water reorientation, *Science*, 2006, **311**, 832–835.
48 H. J. Bakker and J. L. Skinner, Vibrational Spectroscopy as a Probe of Structure and Dynamics in Liquid Water, *Chem. Rev.*, 2010, **110**, 1498–1517.
49 H. J. Bakker, *Chem. Rev.*, 2008, **108**, 1456–1473.
50 M. Ji, M. Odelius and K. J. Gaffney, *Science*, 2010, **328**, 1003–1005.
51 Ł. Szyc, M. Yang, E. T. J. Nibbering and T. Elsaesser, Ultrafast Vibrational Dynamics and Local Interactions of Hydrated DNA, *Angew. Chem., Int. Ed.*, 2010, **49**, 3598–3610.
52 R. Costard, I. A. Heisler and T. Elsaesser, Structural Dynamics of Hydrated Phospholipid Surfaces Probed by Ultrafast 2D Spectroscopy of Phosphate Vibrations, *J. Phys. Chem. Lett.*, 2014, **5**, 506–511.
53 D. Laage, G. Stirnemann, F. Sterpone, R. Rey and J. T. Hynes, Reorientation and allied dynamics in water and aqueous solutions, *Annu. Rev. Phys. Chem.*, 2011, **62**, 395–416.
54 K. Heyne, N. Huse, J. Dreyer, E. T. J. Nibbering, T. Elsaesser and S. Mukamel, Coherent low-frequency motions of hydrogen bonded acetic acid dimers in the liquid phase, *J. Chem. Phys.*, 2004, **121**, 902–913.
55 N. Huse, B. D. Bruner, M. L. Cowan, J. Dreyer, E. T. J. Nibbering, R. J. D. Miller and T. Elsaesser, Anharmonic couplings underlying ultrafast vibrational dynamics of hydrogen bonds in liquids, *Phys. Rev. Lett.*, 2005, **95**, 147402.
56 F. Dahms, R. Costard, E. Pines, B. P. Fingerhut, E. T. J. Nibbering and T. Elsaesser, The Hydrated Excess Proton in the Zundel Cation $H_5O_2(+)$: The Role of Ultrafast Solvent Fluctuations, *Angew. Chem., Int. Ed.*, 2016, **55**, 10600–10605.
57 B. T. Psciuk, M. Prémont-Schwarz, B. Koeppe, S. Keinan, D. Xiao, E. T. J. Nibbering and V. S. Batista, Correlating Photoacidity to Hydrogen-Bond Structure by Using the Local O–H Stretching Probe in Hydrogen-Bonded Complexes of Aromatic Alcohols, *J. Phys. Chem. A*, 2015, **119**, 4800–4812.
58 Z. Dega-Szafran and E. Dulewicz, Infrared and 1H Nuclear Magnetic Resonance Studies of Hydrogen Bonds in Some Pyridine Trifluoroacetates and their Deuteriated Analogues in Dichloromethane, *J. Chem. Soc., Perkin Trans. 2*, 1983, 345–351.
59 V. Balevicius, K. Aidas, I. Svoboda and H. Fuess, Hydrogen Bonding in Pyridine N-Oxide/Acid Systems: Proton Transfer and Fine Details Revealed by FTIR, NMR, and X-ray Diffraction, *J. Phys. Chem. A*, 2012, **116**, 8753–8761.
60 P. M. Tolstoy, B. Koeppe, G. S. Denisov and H.-H. Limbach, Combined NMR/UV-Vis Spectroscopy in the Liquid State: Study of the Geometries of Strong OHO Hydrogen Bonds of Phenols with Carboxylic Acids, *Angew. Chem., Int. Ed.*, 2009, **48**, 5745–5747.
61 B. Koeppe, P. M. Tolstoy, E. T. J. Nibbering and T. Elsaesser, Two-dimensional UV-vis/NMR Correlational Spectroscopy: A Heterospectral Signal Assignment of Hydrogen-Bonded Complexes, *J. Phys. Chem. Lett.*, 2011, **2**, 1106–1110.
62 B. Koeppe, E. T. J. Nibbering and P. M. Tolstoy, NMR and FT-IR studies on the association of derivatives of thymidine, adenosine, and 6-N-methyl-adenosine in aprotic solvents, *Z. Phys. Chem.*, 2013, **227**, 723–749.
63 (*a*) N. V. Drichko, G. Y. Kerenskaia and V. M. Schreiber, Medium and temperature effects on the infrared spectra and structure of carboxylic acid–pyridine complexes: acetic acid, *J. Mol. Struct.*, 1999, **477**, 127–141; (*b*) K. Takei, R. Takahashi and T. Noguchi, Correlation between the Hydrogen-Bond Structures and the C═O Stretching Frequencies of Carboxylic Acids as Studied by Density Functional Theory Calculations: Theoretical Basis for Interpretation of Infrared bands of Carboxylic groups in Proteins, *J. Phys. Chem. B*, 2008, **112**, 6725–6731; (*c*) G. V. Gusakova, G. S. Denisov and A. L. Smolyansky, On νCO Frequencies in IR Spectrum of Non-Symmetrically Perturbed Carboxylate Ion, *Opt. Spectrosc.*, 1972, **32**, 922–925.
64 D. Heckmann, A. Meyer, B. Laufer, G. Zahn, R. Stragies and H. Kessler, Rational Design of Highly Active and Selective Ligands for the $\alpha5\beta1$ Integrin Receptor, *ChemBioChem*, 2008, **9**, 1397–1407.
65 C. Mundy, F. Mohamed, F. Schiffman, G. Tabacchi, H. Forbert, W. Kuo, J. Hutter, M. Krack, M. Iannuzzi and M. McGrath, CP2K, http://www.cp2k.org/, 2000.
66 G. Lippert, J. Hutter and M. Parrinello, A hybrid Gaussian and plane wave density functional scheme, *Mol. Phys.*, 1997, **92**, 477–487.
67 S. Grimme, Semiempirical GGA-type density functional constructed with a long-range dispersion correction, *J. Comput. Chem.*, 2006, **27**, 1787–1799.
68 A. D. Becke, Density-functional exchange-energy approximation with correct asymptotic behavior, *Phys. Rev. A: At., Mol., Opt. Phys.*, 1988, **38**, 3098–3100.
69 C. Lee, W. Yang and R. G. Parr, Development of the Colle-Salvetti correlation-energy formula into a functional of the electron density, *Phys. Rev. B: Condens. Matter Mater. Phys.*, 1988, **37**, 785–789.
70 S. Goedecker, M. Teter and J. Hutter, Separable dual-space Gaussian pseudopotentials, *Phys. Rev. B: Condens. Matter Mater. Phys.*, 1996, **54**, 1703–1710.
71 G. Bussi, D. Donadio and M. Parrinello, Canonical sampling through velocity rescaling, *J. Chem. Phys.*, 2007, **126**, 014101/1.
72 M. J. Frisch, G. W. Trucks, H. B. Schlegel, G. E. Scuseria, M. A. Robb, J. R. Cheeseman, G. Scalmani, V. Barone, B. Mennucci, G. A. Petersson, H. Nakatsuji, M. Caricato, X. Li, H. P. Hratchian, A. F. Izmaylov, J. Bloino, G. Zheng, J. L. Sonnenberg, M. Hada, M. Ehara, K. Toyota, R. Fukuda, J. Hasegawa, M. Ishida, T. Nakajima, Y. Honda, O. Kitao, H. Nakai, T. Vreven, J. A. Montgomery Jr., J. E. Peralta, F. Ogliaro, M. Bearpark, J. J. Heyd, E. Brothers, K. N. Kudin, V. N. Staroverov, R. Kobayashi, J. Normand, K. Raghavachari, A. Rendell, J. C. Burant, S. S. Iyengar, J. Tomasi, M. Cossi, N. Rega, J. M. Millam, M. Klene, J. E. Knox, J. B. Cross, V. Bakken, C. Adamo, J. Jaramillo, R. Gomperts, R. E. Stratmann, O. Yazyev, A. J. Austin, R. Cammi, C. Pomelli, J. W. Ochterski, R. L. Martin, K. Morokuma,

V. G. Zakrzewski, G. A. Voth, P. Salvador, J. J. Dannenberg, S. Dapprich, A. D. Daniels, Ö. Farkas, J. B. Foresman, J. V. Ortiz, J. Cioslowski and D. J. Fox, *Gaussian 09, Revision A.02*, Gaussian Inc., Wallingford CT, 2009.

73 W. Humphrey, A. Dalke and K. Schulten, VMD: visual molecular dynamics, *J. Mol. Graphics*, 1996, **14**, 33–38.

74 M. Brehm and B. Kirchner, TRAVIS – A Free Analyzer and Visualizer for Monte Carlo and Molecular Dynamics Trajectories, *J. Chem. Inf. Model.*, 2011, **51**, 2007–2023.

75 K. L. Schuchardt, B. T. Didier, T. Elsethagen, L. Sun, V. Gurumoorthi, J. Chase, J. Li and T. L. Windus, Basis Set Exchange: A Community Database for Computational Sciences, *J. Chem. Inf. Model.*, 2007, **47**, 1045–1052.

76 D. Feller, The role of databases in support of computational chemistry calculations, *J. Comput. Chem.*, 1996, **17**, 1571–1586.

77 C. Adamo and V. Barone, Toward reliable density functional methods without adjustable parameters: The PBE0 model, *J. Chem. Phys.*, 1999, **110**, 6158–6170.

78 W. Kutzelnigg, U. Fleischer and M. Schindler, *Deuterium and Shift Calculation*, Springer Berlin Heidelberg, 1991, vol. 23, p. 165.

79 The majority of pKa values comes from the *CRC Handbook of Chemistry and Physics*, ed. D. R. Lide, CRC Press, Boca Raton, 84th edn, 2004; B2 and B20: D. D. Perrin, *''Dissociation Constants of Organic Bases in Aqueous Solution (Supplement 1972)''*, Butterworths, London, 1972 Calculated values for B7, B8, B15 were taken from ACS SciFinder.

80 J. Kalenik, I. Majerz, L. Sobczyk, E. Grech and M. M. M. Habeeb, ^{35}Cl Nuclear Quadrupole Resonance and Infrared Studies of Hydrogen-bonded Adducts of 2-Chloro-4-nitrobenzoic Acid, *J. Chem. Soc., Faraday Trans. 1*, 1989, **85**, 3187–3193.

81 M. Tamres, S. Searles, E. M. Leighly and D. W. Mohrman, Hydrogen Bond Formation with Pyridines and Aliphatic Amines, *J. Am. Chem. Soc.*, 1954, **76**, 3983–3985.

82 O. F. Mohammed, D. Pines, E. Pines and E. T. J. Nibbering, Aqueous bimolecular proton transfer in acid–base neutralization, *Chem. Phys.*, 2007, **341**, 240–257.

83 H.-H. Limbach, P. M. Tolstoy, N. Perez-Hernandez, J. Guo, I. G. Shenderovich and G. S. Denisov, OHO Hydrogen Bond Geometries and NMR Chemical Shifts: From Equilibrium Structures to Geometric H/D Isotope Effects with Applications for Water, Protonated Water and Compressed Ice, *Isr. J. Chem.*, 2009, **49**, 199–216.

84 P. M. Tolstoy, P. Schah-Mohammedi, S. N. Smirnov, N. S. Golubev, G. S. Denisov and H.-H. Limbach, Characterization of Fluxional Hydrogen-Bonded Complexes of Acetic Acid and Acetate by NMR: Geometries and Isotope and Solvent Effects, *J. Am. Chem. Soc.*, 2004, **126**, 5621–5634.

85 S. Sharif, G. S. Denisov, M. D. Toney and H. H. Limbach, NMR Studies of Solvent-Assisted Proton Transfer in a Biologically Relevant Schiff Base: Towards a Distinction of Geometric and Equilibrium H-Bond Isotope Effects, *J. Am. Chem. Soc.*, 2006, **128**, 3375–3387.

86 S. O. Morgan and H. H. Lowry, Dielectric polarization of some pure organic compounds in the dissolved, liquid, and solid states, *J. Phys. Chem.*, 1930, **34**, 2385–2432.

87 A. Hacura, Anisotropy of molecular reorientation in liquid methylene chloride, *J. Mol. Liq.*, 1992, **54**, 33–38.

88 J. Hunger, A. Stoppa, A. Thoman, M. Walther and R. Buchner, Broadband dielectric response of dichloromethane, *Chem. Phys. Lett.*, 2009, **471**, 85–91.

89 M. Thomas, M. Brehm, O. Hollóczki, Z. Kelemen, L. Nyulászi, T. Pasinszki and B. Kirchner, Simulating the vibrational spectra of ionic liquid systems: 1-ethyl-3-methylimidazolium acetate and its mixtures, *J. Chem. Phys.*, 2014, **141**, 024510.

90 Dielectric constant of chloroform is *ca.* 4.7 *vs.* that of dichloromethane 8.8 at room temperature: the values of the latter increase more strongly with decreasing temperature; for the reference see *CRC Handbook*, full reference in ref. 79.

91 S. Piana, D. Sebastiani, P. Carloni and M. Parrinello, Ab Initio Molecular Dynamics-Based Assignment of the Protonation State of Pepstatin A/HIV-1 Protease Cleavage Site, *J. Am. Chem. Soc.*, 2001, **123**, 8730–8737.

